Revision 1

VNIR spectral variability of the igneous stratified Stillwater Complex: a tool to map lunar highlands

Carli, Cristian[1], Serventi, Giovanni[2], Sgavetti, Maria[2]

1) Istituto di Astrofisica e Planetologia Spaziali-INAF Roma, Via fosso del cavaliere 100, 00133, Rome, Italy (cristian.carli@iaps.inaf.it)

2) Dipartimento di Fisica e Scienze della Terra, Macedonio Meloni, Università degli studi di Parma, Italy

Abstract

Lunar Highlands are plagioclase-rich terrains produced by crystal floating in a Magma Ocean system. Lunar samples revealed the presence of anorthositic (plagioclase >90%) samples from the Highlands, associated to more mafic rocks. Recently, remote sensing data permits to map those terrains with high spatial and spectral resolution allowing to detect plagioclase and mafic crystal field (C.F.) absorptions.

In this paper we have studied bidirectional spectral characteristics in the visible near-infrared (VNIR) of rocks from the Stillwater Complex, a cumulitic igneous stratified complex, with composition varying from mafic to sialic (e.g. pyroxenite, anorthosite). We investigated both slabs and powders of these rocks to give indication of the spectral variability of rocks analogues of lunar crust, from a mineralogical point of view. Samples have been spectrally separated in four main groups considering the different C.F. absorption association, reflectance and spectral shape for both slab and powder spectra. More spectral details can be obtained from the analysis of powder spectra than from the slab spectra.

The composition of rocks can be addressed by studying spectral parameters, as the position and the intensity of the absorption (e.g. band center and band depth). The analysis of our plagioclase-

pyroxene bearing samples indicates that mafic composition can be clearly obtained for samples characterized by one pyroxene phase, even for few amounts of pyroxene, from powder spectra. On the other hands, slab spectra show clear pyroxene absorptions only for rocks with mafic abundance at least > 20%. The intensity of the mafic absorptions of these samples shows a linear trend with respect to the abundance of pyroxenes (orthopyroxene + clinopyroxene, for samples with ferrosilite amount < ca.25%). Considering all pyroxene bearing samples the band depth of slab spectra are linearly related to the volumetric distribution of ferrous iron in pyroxenes.

Key words: LUNAR AND PLANETARY STUDIES: terrestrial anlogues - OPTICAL SPECTROSCOPY: VNIR reflectance spectroscopy - SURFACE STUDIES: highlands particulate and rocks analogues

Introduction

Lunar highlands have been long considered the product of global Magma Ocean (MO) which produced a wide variety of mafic lithologies in a heterogeneous mantle and a ferroan anorthosite primary crust via the crystallization and floatation of plagioclase (e.g. Smith et al., 1970; Wood et al., 1970; Warren, 1985). It is generally accepted that this body was largely molten during its early evolution (e.g. Warren, 1985), and that the lunar magma ocean (LMO) crystallized from the cooling of the outer portion to form the early crust and the upper mantle (e.g. Warren, 1985).

In particular, lunar surface lithology analyses have been often successful in placing the different rocks in the context of the LMO paradigm (Elardo et al., 2012) even if inconsistencies have been advanced by several authors (e.g. Walker, 1983; Longhi and Ashwal, 1985), pointing out e.g. that several models for the evolution of LMO did not take into account the fact that lunar monomineralic rocks are rare (Snyder et al., 1992). Snyder et al. (1992) modeled the crystallization for the LMO

suggesting an early transition from olivine, orthopyroxene, to calcic pyroxene (ceasing olivine crystallization). After 65-70% of the LMO crystallized, plagioclase came on the liquidus and began to crystallize. This sequence is supposed to be formed from bottom to up the layering of the upper mantle and the crust of the Moon. Similar mineral assemblages sequences are recognized in the layered igneous intrusions on the Earth (e.g. Stillwater complex, Duluth Gabbro Complex, Skaaergard intrusion, Snyder et al., 1992). Warren (1985) also evidenced as crystallization of the LMO can produce a wide variety of mafic lithologies in a heterogeneous mantle with the formation of a ferroan anorthosite crust via flotation of plagioclase rich cumulates.

Recently, data from the multiband imager (M.I.) and the spectral profiler (S.P.) onboard the Japanese SELENE missions and from the Moon Mineralogy Mapper (M^3) Nasa-reflectance spectrometer onboard the Indian Chandrayaan spacecraft, have clearly highlighted as C.F. absorption band close to 1.2 μm is unambiguously recognizable in different regions on the lunar crust and is assignable to ferrous iron in plagioclase (Ohtake et al., 2009; Yamamoto et al., 2012; *Donaldson Hanna et al., in review*). Moreover, it has been evidenced that regions close to pure anorthosites show spectral variation similar to those of plagioclase-pyroxene mixtures with variable amount of mafic minerals (Matsunaga et al., 2008; Ohtake et al., 2009; Cheek et al., 2011; Pieters et al. 2011; Kramer et al., 2013).

M^3 data also revealed distinctive rock-types along the inner basin ring in the Moscoviense (Pieters et al., 2011), designated as "OOS" and dominated by high concentrations of orthopyroxene, olivine, and Mg-rich spinel. These lithologies occur as small areas, each a few km in size, but widely separated within the highly feldspathic setting of the basin rim. Although the abundance of plagioclase is not well constrained, OOS have been classified as pyroxenites and harzburgites due to high mafic mineral content (Pieters et al., 2011). OOS origin appears to be related to one or more magmatic intrusions into the lower crust, perhaps near the crust/mantle interface. The authors hypothesized that processes such as fractional crystallization and gravity settling may provide a

mechanism that concentrate the mafic components within zones several km in dimension. The OOS are embedded within highly anorthositic material; they may be contemporaneous with crustal products from the cooling Magma Ocean (Pieters et al., 2011).

Even if M^3, SP and MI data improved the knowledge of lunar composition, the formation mechanisms of the lunar crust are still a matter of debate and the determination of the highland mineralogical composition, as well as mineralogical variation within the crust, are important for understanding the formation model and the subsequent evolution of the lithosphere.

On the Earth several large layered intrusions are present and well known from a petrographic/petrologic point of view, e.g. anorthosite kindred intrusion like Bushweld Complex (R.S.A.), Stillwater Complex (Montana, USA), Bierkrejm-Sokndal (Norway). The petrographic and compositional variations of these intrusions are expression of their petrology and evolution. Studying spectral characteristics of well-known terrestrial layered intrusions with petrographic and compositional characteristics similar to the lunar crust could be a useful tool to improve spectroscopical and compositional knowledge from remote sensing analysis.

In this paper we have studied samples from different layers belonging to the Stillwater Complex. discussing the spectral variability of rocks from different layers and classifying spectra signature of both powders and cut-rocks. Even if the lunar surface was considered as characterized by fine materials (see e.g. McKay et al., 1974), the development of high spatial resolution spectrometers, as well as, possible future rover missions, will permit to map pixels with spectrum dominated by exposed rocks (e.g. crater wall). This reason motivated us to study both powders and cut-rocks spectra. Moreover, we quantified spectral parameters and compared them with the different mineral chemistry and assemblages, to emphasize correlation between spectral variability and the mineralogy of rocks genetically related to each other.

Geological setting of Stillwater Complex

The Stillwater Complex (SWC) was emplaced 2.7 Ga BP (see McCallum, 1996), and it crops out on the northern edge of the Beartooth Range, one of the major exposed blocks in the Wyoming Archean Province. Several authors studied the mineralogy, petrography and geochemistry of this cumulitic stratified intrusion in order to investigate the evolution of the system, and the presence of important mineralization (e.g. Page, 1979; McCallum et al., 1980, Raedeke and McCallum 1980; Radeke, 1982; Boudreau and McCallum, 1986; Boudreau and McCallum, 1992; Campbell and Murck, 1993). In particular, Raedeke and McCallum (1980) showed how SWC samples from series with cumulate plagioclase have trends analogues to lunar highlands samples. These trends can be associated to: 1) a basaltic systems approaching a perfect fractional crystallization; and 2) an equilibrium crystallization of trapped intercumulus liquid for very plagioclase rich Series (see their Figure 2,3). Raedeke and McCallum (1980) also evidenced that applying the model derived for SWC rocks they could explained the major elements variations in the ferroan anorthosite. Some authors (e.g., see McCallum, 1996; and references therein) interpreted the formation of anorthosite at SWC as an accumulation of coalescent pl-rich suspension (rockbergs) forming large scale sorting similar to that hypothesized for the lunar highlands (Herbert et al., 1977; Shearer et al., 2006).

In this paper we briefly summarized the variations of major/primary minerals, which can be addressed to recognize co-genetic igneous rocks by VNIR spectral reflectance. The SWC's igneous stratigraphy is subdivided into three major zones (Fig.1b), which from base to top are: the Basal Series (BS, not considered in this paper), the Ultramafic Series (UmS) and the Banded Series (BdS). The BdS are then subdivided in three sub-series, Lower Banded Series (LBdS), Middle Bande Series (MBdS) and Upper Banded Series (UBdS). Each Series has been further subdivided in zones and sub-zones. Series or zones are related to the appearance or disappearance of one or more cumulus minerals. The layering in all the complex varies from centimeter to metric scale.

Figure 1

123 The SWC has been proposed as the results of the presence of two compositionally different source
124 magmas: a MgO and SiO_2 rich magma, which formed the UmS, and a tholeiitic magma from which
125 the BS was originated (McCallum, 1996).

126 1) The UmS can be subdivided in a Peridotite Zone (PZ) and in a Bronzite Zone (BZ). The base is
127 placed at the first appearance of significant amount of cumulus olivine (ol) and the root corresponds
128 with the crystallization of the cumulus plagioclase (pl). The PZ is characterized by sequences of
129 cyclic peridotite-hazburgite-bronzitite units where ol ± orthopyroxene (opx) ± chromite are the
130 cumulus phases (Raedeke and McCallum, 1984). Pl occurs as intercumulus phase within 2 and
131 15%. Massive and disseminated chromite can be present in peridotite layers. The rock textures vary
132 from poikilitic to equigranular.

133 The BZ is the upper zone, it is homogeneous, with the opx as cumulus phase (Jackson, 1961). The
134 intercumulus minerals are pl with small amount of other phases (e.g. clinopyroxene (cpx), quartz,
135 chromite). In the upper zone the intercumulus pl and augite (cpx) became more abundant.

136 In the UmS, Ol vary from forsterite content (Fo, Mg/(Mg+Fe)%) 79 to 90. Mg-rich ol are associated
137 to chromite, whereas Fe-rich ol are present in the lowermost peridotites. Opx vary from enstatite
138 content (En, Mg/(Mg+Fe+Ca)%) 76 to 86 with a general Mg enrichment, and intercumulus cpx are
139 in equilibrium with opx composition. Pl shows anorthitic value (An, Ca/(Ca+Na+K)%) between 75
140 and 80, with few samples showing more albitic or anortitic composition (An from 69 to 86).

141 2) The BdS start when pl becomes a cumulus major constituent of rocks. The LBdS are composed
142 of norite and gabbronorite, with minor amount of ol bearing cumulus that host the Johns-Manville
143 Reef (J-M Reef) a platinoid rich reef. The MBdS are composed of anorthosites, ol-gabbros and
144 troctolites and the UBdS comprise gabbronorites with minor troctolites and norites (McCallum et
145 al., 1986).

a) LBdS are characterized in the lower part by rocks with cumulus opx and pl in cotetic proportion, with 1-10% of cpx in the Norite I zone (N-I) that became a primary cumulus phase in the Gabbronorite I zone (GN-I). Modally graded and rhythmic layering are common. The minerals chemistry is quite homogeneous with opx En75-83 and pl An78-83 (Page and Moring, 1987). Above the GNI zone is the ol-bearing zone I (OB-I) where ol appear as cumulus phase. The upper portion of the LBdS is characterized by a uniform member of norite (N-II) and a gabbronorite zone (GN-II) when augite return as cumulus phase. This layering is best developed in norites and gabbronorites that contain pl in excess of cotetic proportions suggesting that the magma may have been slightly undersaturated in pyroxenes (px) (McCallum, 1986). Pl are still quite homogenous in composition with An 75-77, px shows a slightly Mg impoverishment trend except the upper part of the GN-II. The LBdS finishes with a small OB-II layer, where pillows of troctolite are set in an anorthositic body.

b) The MBdS lithologies have high pl volume (> 82 pl.%) as primary cumulus phase, ol and augite are the other most common cumulus mafic minerals while opx is rare. Therefore, the major lithologies are anorthosite, troctolite, ol-gabbro, and rare gabbronorite (±ol). The difference from the other Banded series is probably due to a change in composition of the magma with respect to the LBdS and UBdS parental magma (Raedeke, 1982; Irvine et al., 1983).

The MBdS starts and finishes with two thick uniform anorthosite zones (An-I and An-II) with the presence of minor amount of oikocrysts or intercumulus crystals of augite, opx or inverted pigeonite. Px-rich and px-poor domains are present in An-I and An-II, suggesting a possible formation due to a coalescence of meter-sized rockbergs of partially consolidated pl cumulates (Haskin and Salpas, 1992). Pl composition are virtually constant with An76-77 on large scale, but are more heterogeneous on a cm scale (McCallum et al., 1980). The central area of the MBdS is characterized by two ol-bearing zones (OB-III, OB-IV) which are formed by troctolites and anorthosites in the lower parts, overlain by ol-gabbro. The uppermost unit in both OB-III and OB-

IV is a ol-gabbronorite where both ol and opx appear to be a cumulus minerals in addition to pl and augite. There is no systematic variation in mineral composition and pl are similar to An-I and -II with an average An77 (McCallum et al. 1980, Meurer and Boudreau 1995). Mafic mineralogy of MBdS show no systematic variation, but a generally iron-richer composition with respect to LBdS and UBdS.

c) The UBdS begin with a banded troctolite (OB-V zone). This zone is characterized by ol-rich lenses along the contact, rising the body shows modally graded layers, cross-bending, scour and fill structures, indicating strong action during the formation. The root of OB-V present a thick anorthosite layer which degrade in a repetitive sequence of anorthosite-norite-gabbronorite. The upper zone of UBdS is a gabbronorite (GN-III). The GN-III starts with a sequence of homogeneous laminated gabbronorite, with pl, augite and low-Ca px in cotetic proportion. The opx result as a cumulus phase in lower part, while in central and upper part it is present as poikilitic crystals derived by the inversion of cumulus pigeonite. In GN-III can be present magnetite as post-cumulus phase, irregular pegmatite zone and xenoliths of anorthosite. Pl shows a change from An75 to An62 rising along the section, as well as, low-Ca px moves from Mg# (magnesium number) 0.75 to 0.67 (Radeke, 1982).

Methods

Twenty samples with different composition have been considered in this work, representing various layers of the complex. Only few samples had a clear indication of the collected site (see Fig.1b and caption). We used the bulk rock composition, mineral chemistry and mineral abundances to correlate the other samples with units (see Fig. 1a,b).

Reflectance spectra were measured on rock powders at different grain size (<0.050, <0.125, <0.250 mm) and on slab samples. The slab samples are considered as analogues of cm size natural rock grains and compact multimineral aggregates in the regolith (Carli and Sgavetti, 2011). Studying

both powders and slabs spectra permit to evidence how varies the influence of the optical coupling with respect to the minerals absorptions. This aspect is very important (interesting reader see also Carli and Sgavetti, 2011) to understand spectral information of multi-crystal grains which can be present in a regolith.

Powder and slab samples were prepared from the rock portion adjacent to the thin section used for petrographic and chemical analyses. On slab (cut surface) samples, the measured surface was slightly polished using a silicon carbide abrasive, having particle sizes in the range between 10 and 20 μm. The abrasion permits the removal of the asperities left by the saw, but does not produce a mirror-like surface. In order to preserve the original rock composition in powdered samples, the rocks were first ground to prepare the <2.00 mm coarse grain size class. The coarse powders were then quartered and each fraction was ground under smaller grain size classes, <0.250 mm, <0.125mm and <0.050 mm. Each powder grain size class therefore contains a range of grain dimensions beneath the upper limit, except for the slab.

Mineral assemblages and rock textures were described through optical microscopy on thin sections. A point counter was used to measure the relative modal abundance of minerals and according to the IUGS Subcommission on Rock Classification (LeMaitre et al, 2002; Le Bas et al., 1986), the intrusive rocks are classified by the relative modal abundance of the primary mineral. Rock chemistry was analyzed using a X-ray fluorescence spectrometer (XRF), in use at the XRF laboratory at Geosciences Department of the University of Padova. The chemistry of the principal mineral phases was determined by electron microprobe analyses with a CAMEBACAMECA SX50 (EMPA) at the microprobe laboratory of C.N.R.-IGG, Padova. The rock modal and chemical compositions and mineral chemistry are reported in tables 1, 2 and 3.

Slab spectra were measured using diffuse reflectance spectroscopy at IFAC-CNR, Florence, using a double-beam double-monochromator spectrophotometer (Perkin-Elmer-Lambda 19) with a 60 mm integrating sphere and an halogen lamp as source of irradiation. Spectral resolution and sampling

was 1 nm between 0.35 and 2.50 μm at room temperature and normal atmospheric pressure. The illuminated spot was ca. 1 cm^2, suitable for characterizing rocks with relatively large crystal sizes. To account for the heterogeneity of the rocks and to assure the spectral and petrographic data comparability, five separate adjacent spots were acquired over about 6-7 cm^2 sample area and averaged. A smoothing function based on a Fast Fourier Transform (FFT) algorithm using twenty data points has been applied to the average spectrum, without significant effects on the diagnostic band minimum positions. Bidirectional spectra of powders at different grain sizes were acquired using a Fieldspec Pro spectrophotometer mounted on a goniometer at S.LAB. laboratory, at "Istituto di Astrofisica e Planetologie Spaziali", IAPS- Inaf, Rome. The spectra were acquired with a spectral resolution of ~3 nm in the VIS and of ~10-12 nm in the NIR, with i=30° and e=0°. The source used was a QTH (Quartz Tungsten Halogen) lamp and the spot illuminated has an area of ca. 0.5cm^2. The standard reference calibration was performed with a Spectralon® optical standard (registered trademark of Labsphere, Inc.) both for slab and powder measurements.

Analytical approach

All the samples were spectrally characterized both as slab of rocks and powders (<0.250 mm) to define a spectral classification. C.F. absorptions representative of the dominant mineral phases (Fig. 2), as well as, spectral shape (defined by the presence of different absorbing phase and the spectra slope) were used to identify the different spectral groups. Three major C.F. absorptions at ~ 1.00, 1.25, 2.00 μm, were labeled as Band I, V, and II; very weak IVCT (intervalence charge transfer) bands (Band III, IV) were identified at ~ 0.55-0.65 μm. Some samples also show overtone absorptions, at ~1.4, 1.9, 2.2-2.3μm, labeled a, b, c, d, due to the presence of mineral alteration, like epidote, serpentine, bowlingite, iddingsite.

Figure 2.

We then compared the spectral classification with mineral and rock compositions (see section 6.1).

Subsequently for each C.F. absorption we determined band center (B.C.) and band depth (B.D.), after continuum removal by division; and considering a wavelength's function continuum line as segments that join the reflectance maxima in the spectrum (Clark and Roush, 1984). The reflectance maxima are chosen for each samples depending on the single spectrum, they vary from 5 to 8 points. The B.C. results in the position of the minimum of each absorptions after the continuum removal, and the B.D. is the difference between the continuum reflectance and the B.C. reflectance after the division with the continuum (Clark and Roush, 1984). In particular, we refer to B.C.I and B.D.I for the position and intensity of Band I, and to B.C.II and B.D.II for the Band II. For selected samples characterized primary by pl, opx and cpx we measured spectra of finer grain size, <0.125 mm and <0.050 mm, to consider sizes closer to a fine regolith.

The B.C. and B.D. of slab and powder spectra were correlated to mineral and rock composition to analyze trends and investigate differences between slab and powders spectra and within different grain size for samples dominated by plagioclase and pyroxenes. In particular, B.C. of C.F. absorptions can be directly associated with the Fe^{2+} amount on silicates (e.g. ferrosilite content, Fs%, Fe/(Fe+Mg+Ca), in Cloutis and Gaffey, 1991; Klima et al., 2007; Fa/Fo% in Burns, 1993) or indirectly to Ca^{2+} (e.g. px band I and II in Cloutis and Gaffey, 1991); here we related the absorption position to Fs% and Wo% (wollastonite content, Ca/(Fe+Mg+Ca)) to compare the data with Cloutis and Gaffey (1991). B.D. of px-bearing rocks has been plotted vs. the px abundance and vol.Fe^{2+} in px, to highlight if the variation in composition of mafic minerals can influence the known relationship between B.D. and mineralogy (similarly to e.g. Pompilio et al. 2007).

The Stillwater Complex: mineralogy and petrographic characteristic of investigated samples

Petrographic observation under optical microscope were made for twenty samples, recognizing mineral phases and relative abundances. Mineral chemistry and bulk rock were also measured to obtain information useful to discuss the VNIR spectral variations and to constrain the unit of provenance of some samples (see Fig. 1).

Seven samples (StC1, StC2, StC3, StC4, StC5, StC6, StC7) representative of the UmS, are characterized by cumulus of mafic phases (ol, opx) ± chromite, while pl and cpx (augite) are present as intercumulus or postcumulus phases. Mineral phases show low amounts of hydrated alteration. StC2,4,7 are mela-norites (Fig.3) with high amount of cumulus opx, and a small amount (~13%, see table 1) of cumulus ol in StC2. StC1,3,5,6 are characterized by relative higher abundance of cumulus ol and a variable but significative presence of cumulus opaque minerals (chromite). StC1 and StC5 present a poikilitic texture with opx crystals present as oikocrysts surrounding small cumulus ol. Chromite abundance vary from 2% (StC5) to 28% (StC1) to 55% (StC6) to 90% (StC3).

Figure 3.

Other samples are representative of the BdS. Pl is a cumulus phase, present with variable amount, in association with mafic minerals, which can be cumulus or intercumulus crystals. On the base of mineral association, samples can be divided in:

Anorthosites (StC9,10,18), very pl-rich rocks (relative pl>90%), with few amount of intercumulus cpx, and opx in StC10. Zoisite is present in StC9 and StC18 as plagioclase alteration;

Leuco-gabbros (StC11,13), very similar to anorthositic samples but with an higher amount of cpx. In StC13 is also present low amount of opx either as intercumulus crystals or as exolution in cpx;

Gabbronorites (StC8,12,14), characterized by the presence of high amount of cumulus pl and different opx/cpx ratio. Opx are generally cumulus whereas cpx can be either small cumulus or intercumulus phase;

Mela-norites (StC20,25), characterized by high, iron-bearing opx amount as cumulus phases. Despite the relative low amount of pl, the ratio between Mg# of opx and An of pl suggests that they are compatible with BdS composition (Fig. 2);

and Ol-bearing samples (StC16,17,19), characterized by high amount of pl and an amount of cumulus ol higher than opx+cpx. StC17 and StC19 present high degree of ol alteration (serpentine); moreover, StC17 have pl partially altered (epidote).

Figure 4 shows the general variation of the mineral chemistry. Opx varies from En91 to 61, with Mg richer samples from UmS; this variation is recognized also in cpx composition (with En from 48 to 39, and Wo 45 ±1) and in ol with Fo increasing from 88 for UmS to 76 BdS. Pl shows a composition from An70 to An89, with An79-89 for BdS. Moreover pl chemistry shows a variable FeO from 0.1 wt.% to 0.5 wt.%, from mafic rich to pl rich rocks, respectively.

Figure 4.

The Stillwater Complex: VNIR spectroscopy results

Spectral classification

We spectrally classified all the samples consisting of rock powders (<0.250 mm), to consider spectral characteristics of natural-mixtures of mono-crystal grains (Fig. 5), and spectra measured on slabs, to consider spectral characteristics of multi-crystals grains (Fig. 6) (*see also Carli et al., in press*). This spectral classification of the SWC samples is based on C.F. absorptions of the primary minerals (px, ol, pl, chromite) and, secondary, considering also the spectral slope and reflectance.

Powders spectra (Figure 5) can be classified in four main groups, further subdivided into subgroups, as follows:

1) The first group (Group 1_p, Fig. 5a) is characterized by a wide absorption band at ~1.25 μm (Band V) and high albedo. These samples are pl-rich rocks, two anorthosites and a leuco-gabbros (StC 9, 18 and 11, respectively, see Table 1), which have cpx as only mafic phase. Vibrational bands are indicative of zoisite.

2) The second group (Group 2_p, Fig. 5b) is dominated by the two absorption band at 1.00 and 2.00 μm indicative of px. In figure the reflectance is scaled, for clarity, but spectra are ordered from bottom to top following the reflectance (maximum at ca. 0.75 μm vary from 0.27 (StC25) to 0.46 (StC10)) and the spectral contrast is maintained. This group can be further divided into two subgroups: the Group 2a_p whit spectra characterized by the band I and II, it is the most populated group; the Group 2b_p (grey labels) show the two px absorptions and the evidence of the bandV absorption, indicative of pl. The Group 2b_p is characterized by the samples within the second group with the highest amount of pl, and both cpx and opx (StC10,13,14), which have the highest albedo and the lowest px absorption's spectral contrasts. Gabbronorite spectra (samples StC8,12,14) are characterized by px composite bands, with position and asymmetry correlated to the opx/cpx ratio. Some spectra show small vibrational bands indicative of very small amount of alterations. In the visible range are also present weak IVCT absorptions.
3) The third group is defined by a wide absorption band from 0.5 to 1.7 μm (Fig.5c, Group 3a_p). StC16 shows a lower spectral contrast due to its modal distribution, when Fe^{2+} is present in several minerals (e.g. pl, opx, cpx and ol) the contribution of all of this absorbing phases in contiguous wavelength range reduce the contrast of the composite absorption (Carli and Sgavetti, 2011, see their fig. 3,5); whereas StC5 is characterized by a defined absorption related to Fe^{2+} in M1 and M2 site of ol (Burns, 1993). Both samples are composed of fresh ol. In the Group 3b_p are present spectra with very low albedo and spectral contrast, and C.F. absorption features only suggested by a weak inflection centered at about 1.05 μm, representing samples containing strongly serpentinized ol.
4) The fourth group (Fig. 5d) included spectra dominated by low albedo and a clear influence of chromite at wavelength higher than 2 μm. This group can be subdivided into two groups. One is characterized by chromite dominated sample (StC6, Group 4a_p). In Group 4b_p are

present StC1 and StC3 spectra showing two absorption bands at 1 and 2 μm, although weaker then spectra in the second group, reflectance lower than 0.2, and the clear influence of chromite at wavelength higher than 2 μm (absence of a band shoulder around 2.4-2.5 μm).

Figure 5.

Slab spectra can similarly be subdivided into four main groups on the basis of absorption band association and overall reflectance and spectral contrast (Figure 6). However, the different processes acting in the bulk samples with respect to the powder samples affect in different ways albedo, spectral contrast and spectral slope, resulting in different spectral class populations for the two sets of spectra, particularly for the first two groups.

1) The first group (Group 1_s) is identified by a wide absorption band with a minimum close to 1.25 μm (BandV), high albedo (Fig. 6a, albedo max in the visible from 0.35 to 0.55), and a general blue slope, typical of slab spectra. The wide absorption band at ~1.25 μm is indicative of Fe^{2+} in pl (Burns, 1993). These samples in fact are pl-rich rocks and include three anorthosites (StC9,10,18) and two leuco-gabbros (StC11,13)(see Table 1). StC10,13 (opx-bearing samples) were not included in the corresponding Group 1_p. Vibrational bands are present indicative of the small amount of pl's alteration, like epidote or sericite.
2) The second group (Fig. 6b) is still the most populated. The spectra are characterized by the presence of a well developed absorption band or a clear flexures at 1.00 μm associated to a wider and weaker band or a subtle flexure in the 2.00 μm region indicative of px (Burns, 1993). The spectra also show intermediate to low albedo. This group can be split into two subgroups on the basis of the 1 μm feature, the spectra with clear band I absorption are in Group 2a_s (black labels) and spectra with band I flexure are in Group 2b_s (grey labels). The Group 2b_s includes two gabbronorite samplesStC8 and StC14, whereas a third

363 gabbronorite, StC12 (Group 2a_s), show clear absorptions. The different spectral behaviors
364 could be related more with some petrographic variation (e.g. different plagioclase crystal
365 sizes distributions) than with mineralogical characteristics (abundance or chemistry), which
366 affects and complicates the optical path of the light. This aspect, not discussed in details
367 here, is object of ongoing work. Some spectra show weak vibrational bands indicative of
368 very small amount of alterations. In the visible range are also present IVCT indicative of
369 Fe^{2+}-Fe^{3+} or Fe^{2+}-Ti^{4+}.

370 3) The third group is characterized by intermediate to low albedo spectra with very subtle
371 spectral features. However, also these problematic spectra can be tentatively included into
372 two subgroups. Group 3a_s includes spectra in which a shallow absorption or flexure can be
373 recognized in the C.F. region from 0.5 to 1.75 μm (Fig. 6c, StC5,16). These spectra
374 represent ol bearing samples. Group 3b_s includes two featureless spectra characterized by a
375 blue, almost flat, slope. They represents strongly altered (StC19) or completely
376 serpentinized (StC17) ol-bearing samples.

377 4) The fourth group shows low albedo (<0.12) spectra with a broad, weak absorption at 2 μm
378 towards longer wavelength (Group 4a_s). These samples are characterized by high chromite
379 abundance (Fig.6d). Samples StC6 shows also an absorption at ca. 1.1 μm, as for powder
380 spectrum (see Group 4a_p), which can be indicative also of ol. Group 4b_s: sample StC1,
381 with almost 90% of chromite, still show, even if weak, a clear band I absorption, with a
382 band II broad toward longer wavelengths than those seen for px in Group 2a,b_s.

383 Figure 6.

384 **Spectral parameters**

385 The strong blue slope that affect all slab spectra prevent the reliable recognition of the band II long
386 wavelength shoulder, thus only the B.C.I and B.D.I parameters were considered (see Fig.5,6). In

387 contrast, powder samples B.C.II and the B.D.II parameters were analyzed, even if some spectra
388 appear to be highly affected by the presence of alteration mineral phases, as indicated by the 1.9 μm
389 overtone band (υ1+ υ2).

390 In the literature, several papers indicate how mineral and mineral mixture composition can be
391 related to the spectral parameters variations, as: 1) the B.C. absorption bands at 1 or 2 μm was
392 related to px chemistry, stated as Fs or En content and Wo content (e.g. Cloutis et al., 1991; Burns,
393 1993; Sunshine et al., 1991; Klima et al 2007; 2011); 2) ol B.C. is a function of Fo-Fa value (Burns,
394 1970; Cloutis et al. 1986); 3) the B.C. at ~1.25 was assigned to Fe^{2+} in pl with position varying with
395 the amount of iron in the crystal structure (Bell and Mao, 1973; Serventi et al., 2013). Mineral
396 abundances have been successfully related to the band intensity (expressed as B.D. or Band Area)
397 for different type of mixtures. Cloutis et al. (1986) found a linear relationship between Band Area
398 Ratio (Band II Area/Band I Area; BAR) vs. px/(px+ol) for some px-ol mixtures. Pompilio et al.
399 (2007) described as B.D. of opx mixed with pl or dark materials varies linearly with the relative
400 abundance of opx, and a similar behavior was expressed by the B.D.I of slab spectra of rocks
401 characterized by opx± pl, ilmenite. Serventi et al. (2013) studying mixtures of pl and mafic material
402 demonstrating the unexpected spectroscopic effects of PL chemistry superimposed on the expected
403 effects due to modal composition in these mineral mixtures. Moreover, Serventi et al. (2013)
404 pointed out that B.D.I for opx rich end members shows linear variation vs. the amount of
405 volumetric iron in pl.

406 So, B.C. is often related to mineral chemistry, here we considered a weighted Fs% and Wo% value,
407 that is a weighted content of the Fs and Wo of both pyroxenes in samples (e.g. $cpx\%*Fs\%^{cpx}$ +
408 $opx\%*Fs\%^{opx}$), in order to partially compare our results with Cloutis and Gaffey (1991).
409 Figure 7 shows the B.C.I variation vs. the Fs% weighted for all the grain sizes. In particular, Fig. 7a
410 displays the band center for the <0.050 mm class and three fields can be recognized: 1) StC2, 4, 7, 8
411 and 12, centered between 0.9 and 0.93 μm, indicate opx-rich samples (opx/cpx>1) and the center

412 moves to longer wavelength with increasing Fs%, with the exception of StC12, composed with
413 considerable amount of cpx ; 2) StC10, 13 and 14 are centered at longer wavelength, 0.95-0.98 μm,
414 due to the opx/cpx<1. In this field there is not a clear variation trend with mafic composition; 3)
415 StC18, opx-free, is centered at 1.05 μm. Fig. 7b compares the <0.050 and <0.125 mm classes,
416 showing that coarsening the grain size B.C.I slightly move towards longer wavelength (as seen also
417 e.g. by Serventi et al. 2013 for mafic and pl phases, and Clenet et al., 2011 for ol). The shift is very
418 reduced for samples with almost mono px phase, whereas is higher in samples belonging to the
419 second field (St13, 10 and 14). Fig. 7c shows that, with the exception of StC18, the position
420 difference between the <0.125 and the <0.250 mm classes is strongly reduced. In the figure are also
421 plotted the ol-rich sample (StC5, 16) centers that fall in the third field. StC20 and 25 are composed
422 with very high amount of iron-rich opx: the centers fall in the first field but the wavelength are
423 lower than expected, probably due to the saturated bottom-flat absorption band. Fig. 7d finally
424 shows the behavior of slab spectra: centers are at shorter wavelength with respect to the 0-250 μm
425 powders (with the exception of StC20, 25), probably due to the saturation effect in slabs (see Carli
426 and Sgavetti, 2011). Fig. 7d also shows the pl-rich samples (StC10,13,18,9,11), centered at longer
427 wavelength than the px-rich samples, between 1.20 and 1.30 μm, due to the strongly influence of pl
428 absorption on coarsest grain sizes.
429 Figure 7.

430 Figure 8 shows the B.C.I vs. the weighted Wo%. In particular it shows that: 1) with increasing the
431 Wo% content, B.C.I generally moves to longer wavelength, from the opx-rich samples to the cpx-
432 rich (StC10, 13, 14 and 18); 2) coarsening the powders grain size, centers move toward longer
433 wavelength; and 3) St5 and 16, representative of ol-rich samples, fall outside the variation trend.
434 Figure 9 shows the B.C.II vs. the Fs% (Fig. 9a) and Wo% (Fig 9b) weighted for all the powder
435 grain sizes. Several samples show position centered at about 1.9 μm, due to the vibrational
436 processes indicative of alteration superimposed to the px C.F. absorptions. Only some opx-rich

437 samples have B.C.II no affected by the 1.9 μm, those samples show a clear trend respect Wo% for
438 values <5% (see Fig. 9c).

439 Figure 8.

440 Figure 9.

441 B.D. is the expression of the intensity of the absorption band, which is related to the probability of
442 electronic transitions between different crystal field states occur (Burns, 1993). This parameter
443 depends on different chemical and physical properties which affect the optical absorption. In
444 particular it can be affected by: variation in the abundance of the absorbing elements in a mineral
445 (e.g. Fe^{2+} in px); variation of ratio between minerals in a mixture (e.g. opx/cpx); and variation of
446 grain or particle sizes. Because all of these aspect are acting on the B.D. with different contribution
447 in our paper we have considered the variation of B.D. with respect to the mineral abundance and
448 considering the Fe^{2+} influence. For this reason, B.D.I and II are plotted vs. the abundance of px
449 (Fig. 10a,b and Fig. 11a) and vs. the volumetric Fe^{2+} in px (Fig. 10c,d and Fig. 11b). Moreover we
450 have plotted it for the different studied grain sizes.
451 B.D.I of powder spectra shows a linear trend with very high correlation vs. the Opx%+Cpx%
452 (Fig.10a) with angular coefficient similar for different grain sizes (0.0054 to 0.006). Also, B.D.I
453 increases with coarsening the powder size, while it decreases in slabs. Including the iron-richer
454 samples (StC20 and St25) for the <0.250 mm size, values are still correlated (Fig. 10b). Slab spectra
455 show a linear relationship with a lower confidence (R^2=0.71 with respect to R^2 >0.94 for powders)
456 and a very low angular coefficient (0.0025). Considering StC20 and StC25, R^2 further diminishes to
457 0.65 due to the saturated px absorption.
458 In Figure 10c, B.D.I shows a liner relationship with very high coefficient value (0.93 for slab and
459 0.98 for finest powders) with respect to vol.Fe^{2+} in px; however, Fig. 10d shows that powder
460 samples with grain size <0.250 mm show a worse R^2 (0.76) when we include the iron-rich px

461 bearing StC20 and StC25 samples and can be better fitted with a second degree polynomial relation,
462 with a R^2 of 0.86.

463 Figure 10.

464 In figure 11, B.D.II shows linear relationships with a slightly lower R^2 value for <0.250 mm grain
465 size considering iron rich px spectra with respect to selected samples.

466 Figure 11.

467 **Discussion**

468 1) Stillwater Complex samples show a high variation of pl/mafic material and both pl and mafic
469 minerals have variable chemistry among layers of the plutonic system. Figure 12 shows the pl/mafic
470 variation for all samples; even if pl-mafic composition in SWC samples varies, the trend of mineral
471 abundance with respect to sample's Fe_{tot} are comparable to those of mineral mixtures studied by
472 Serventi et al. (2013; see their Fig. 2). In particular, Fig.12b shows that pl-rich rocks contain the
473 iron-richest pl, while mafic-rich samples consist of the iron-poorest pl.

474 Figure 12.

475 A rock powder spectrum, though different from that of a mineral mixture with the same chemistry
476 and modal composition as the rock, however often displays the diagnostic absorption bands of the
477 most abundant component minerals. The spectra measured on samples of a rock suite as the
478 intrusive Stillwater Complex can be usefully classified into groups, each including spectra with
479 same association of absorptions or spectral shape. This provides a "spectral classification" that
480 facilitates the comparison with the petrographic classification and the correlation with the intrusion
481 stratigraphy, and, finally, allows the recognition of a "spectroscopic stratigraphy" of the Complex
482 (e.g., Ferrari et al.1996; Longhi et al., 2001). Slab spectra suffer the effects of petrographic
483 characteristics (e.g. crystal size and its distribution, cumulus/intercumulus phases, poikilitic
484 textures, etc.) which strongly influence the slope and absorption spectral contrast, up to even

485 suppress some absorption features. However, bulk rock spectra can contribute to the spectral
486 description of a natural rock suite, adding spectral information needed for the interpretation of
487 remote sensing or in-situ high spatial resolution hyperspectral data.

488 Almost mono-mineralic rocks are characterized by the component mineral phase signature, and the
489 spectral variation is mainly related to the different grain sizes. On the other hand, the spectra of bi-
490 mineral or multi-mineral rocks are characterized by composite bands, due to absorption processes
491 acting on few tens of micron (e.g. opx and augite). Here, we have considered <0.250 mm powder
492 and slab spectra to define the spectral characteristics of samples and pooling in spectral groups
493 depending on C.F. absorption, reflectance and shape. For selected samples, characterized by pl-px
494 association, we have also acquired spectra of smaller grain sizes to discuss spectral parameter
495 variation related to the sizes.

496 2) Both powder and slab spectra have been classified into four predominant spectral groups. Two
497 groups show a dominant C.F. associations (Band V due to pl, Group 1_p,_s, or Band I and II due to
498 px, Group 2a,b_p,_s). The Goup 1_p_s are characterized by samples from BdS. Group 2a,b is
499 composed by samples from both UmS and BdS, with variable px amount and composition (see
500 table 1 and 3). Note that, StC2, despite the presence of 13% of ol, can't be differentiated from the
501 others. Group 2b_p show also the evidenced for a the Band V due to pl over the absorption Band I
502 and II. Group 3a_p,_s is indicative of ol samples (StC5 from UmS and StC16 from BdS) , whereas
503 samples with ol highly altered are featureless (Group 3b_p_s); those samples are from ol-bearing
504 zones of MBdS or UBdS. Group 4a_p,_s is characterized by spinel bearing evidence due to the
505 spinel absorption at circa 2.0 μm towards the infrared (absence of a shoulder at 2.2-2.5 μm
506 wavelength region), a general low reflectance and reduced spectral contrast (Group 4a_p,s). In the
507 Group 4b_p,_s are still present samples with the clear influence of spinel but also Band I and II. All
508 samples of the Group 4 are from UmS.

Although the groups recognized for slab and powders are similar, some differences are evident. Pl rich rocks show clear Band I and II where mafic minerals are present as both opx and cpx for powder spectra (sample StC10,13) while considering slab spectra only Band V is detectable. Group 2a is composed by the same samples for both powder and slab spectra (with the only exception of StC8), as well as, Group 3a and 3b. Group 4 includes samples StC1,3,6 and showing spinel signature. Group 4_p_s are characterized of spectra dominated by the spinel absorption (StC6 for powder and StC3,6 for slab), whereas in Group 4b_p,_s are present spectra with px absorptions influenced by chromite absorption, StC1 and StC3(even if the chromite abundance is > 90%) for powder and only StC1 for slab.

3) The spectral variation of B.C.I, II and V and B.D.I and II, have been quantitatively described by the analysis of spectral parameters, thus allowing the comparison with compositional information in order to quantify the spectral parameters. In the SWC suite, B.C.I variation reflects the mineral chemistry variation even if not all the mineral components can be resolved. Figure 7 shows how samples with one mafic phase (opx or cpx) have band center comparable with px of Cloutis and Gaffey (1991) for the finer powder grain sizes. Opx rich samples have B.C.I comparable to Cloutis and Gaffey (1991) also for <0.250mm, whereas in anorthosite sample StC18, which presents cpx as mafic phase, B.C. is shifted to longer wavelength due to the strong effect of the high pl (94%) abundance. Sample with gabbronoritic composition and opx/cpx > 1 (StC8, StC12) show B.C.I dominated by opx for all the powder grain sizes; samples with opx/cpx < 1 are closer to intermediate cpx (~Wo. 30%, Cloutis and Gaffey 1991) with positions moving to longer wavelength, towards augitic composition, coarsening the grain size. Figure 8 shows as B.C.I in px-bearing samples follows a trend similar to Cloutis and Gaffey (1991) with respect to the Wo%. Both Fig. 7c and Fig. 8 display how powder spectra of StC9-StC11 (BandV) and ol-rich samples (StC5, StC16) are far from px positions, behavior emphasized for slab spectra. Slab spectra also show a shift to slightly longer wavelength even for some px-bearing samples (StC8,20,25).

In particular, in the SWC we observe that coarsening the grain size the composite band absorptions become more affected by most abundant mineral phases, even if less absorbing (e.g. B.C.I move to higher wavelength or is made up by band V). This behavior can be probably related to different optical paths, and different behavior of single mineral phases with respect to the incident light. Pl absorption becomes, generally, more influent for bigger particle size, in agreement with Serventi et al. (2013).

B.D.I of ol-free samples (both including and excluding StC20, 25, Figures 10a,b) show linear relationship (high R^2) with respect to the pxs abundance, with angular coefficient that slightly increases with the grain size (B.D.I are almost identical for all the grain sizes). Considering slab spectra, the B.D.I still varies linearly (even if with lower R^2) and StC20 and StC25 are outliers (Fig. 10a,b). We investigated also the relationship of B.D.I vs. the volumetric Fe^{2+} in pxs: for slabs, it shows a linear relationship with $R^2 = 0.93$, considering all the samples (Fig. 10c), whereas, for powder spectra, the trend is described by second degree law (with R^2=0.86, Fig. 10d).

It has been demonstrated in the literature that slab spectra have lower albedo and reduced spectral contrast (Pompilio et al. 2007, Harloff and Arnold 2001). Consitently, in the SWC sample set the overall reflectance reduction linearly increases with increasing the modal % of absorbing minerals, indicated by the variation of the angular coefficient. Moreover, in slabs spectra we cannot discriminate the px absorptions for samples with less than 20% opx+cpx. Powders B.D.II also shows a linear relationship for all the powders with only StC25 as outlier in coarser powders (fig 11). Even this trend shows a slight increasing of the angular coefficient coarsening the powder size.

The B.D.I and II behavior of powders shows how, despite possible mineral chemistry variations in rocks co-genetically related, the intensity of the absorption is strictly related to the rock composition (mineral abundance, Fig. 10a,b), even if samples with very high iron-rich mafic concentration show band depth slightly higher than predicted (probably rocks from enriched residual magma). The importance of mineral chemistry in addition to the mineral abundance is strongly evidenced on slab

559 spectra which show saturated band minima, resulting in a B.D. linearly related with the ferrous iron
560 volumetric distribution (Fig. 10c). Moreover, B.D. for different grain sizes are almost unchanged,
561 with the band depth slightly increasing coarsening the grain in agreement with the observation of
562 Harloff and Arnold (2001) for similar grain sizes of px or basalts.

563 Integrating the spectral classes with the spectral parameters analysis assigns a geologic significance
564 to the spectral classes. Within each class, the absorption band association and variation of band
565 centers and band depths give information on the rock composition, allowing the correlation with
566 the igneous stratigraphy as derived from field survey. Figure 13 shows the stratigraphic distribution
567 of the spectral classes, based on both powder and slab spectra. We can observe that UmS and LBdS
568 are represented by Group 2 spectra for both powder and slab, with Group 2b_p present in the
569 MBdS. The PZ is also characterized by Group 3a and Group 4 consistently with the alternation of
570 peridotite-harzburigte-bronzitite and with localized layers enriched in chromite. Whereas the Group
571 1 is indicative of the MBdS for slab spectra, and only of the AnI and AnII for powder spectra, due
572 to the plagioclase Band V. Group 3b indicates the ol-bearing layers of the MBdS, which are high
573 altered in serpentine.

574 Figure 13.

575 **Implications**

576 M3 and S.P. analyses revealed that anorthositic lunar highlands can be associated to local regions
577 with high mafic content (e.g. Ohtake et al., 2009; Pieters et al., 2011). Minerals like px, ol, as well
578 as spinels, were detected in lunar samples (see e.g. summary in Lucey et al. 2006) and have been
579 recently mapped by remote sensing data (e.g. Pieters et al., 2011). Spectral signature of the
580 principally rock forming minerals can be described for both rocks and powders with a definition of
581 the rocks variability in the intrusive complex. Mineral composition and mineral abundance

582 variations are useful information that can help to understand if rocks could be associated genetically
583 each-other.

584 SWC samples are representative of a set of the major petrographic and mineral variation present in
585 a layered intrusion. Understanding the VNIR spectra variation will help us to improve our
586 capability to classify and discuss spectral signatures indicative of geological variations on planetary
587 surfaces. In this paper we in particular investigated the spectral variability of an anorthositic
588 kindred. The spectral analysis of a number of both powder and slab samples showed that the
589 spectral variability permits us to classify the rock suite on the basis of the spectral band association,
590 revealing the dominant mineralogy (Fig. 5,6). Powder spectra (similar to a finest regolith) gives
591 more information than slab spectra (representative of coarse regolith, e.g. higher amount of
592 outcrops). Hyperspectral imaging data contains the influence of both composition and physical
593 properties of each pixel. Because the presence of fine to coarse materials influences the
594 compositional analysis, an accurate spectral description associated to a morphological interpretation
595 is needed to avoid wrong "spectral lithology" classification (done considering absorption
596 identification and quantitative absorption analysis, e.g. B.C. and B.D.). Thus hyperspectral imaging
597 analysis will be improved once the correlation of spectral features from fine to coarse material will
598 be better understood.

599 In our work we have shown how B.C.I is closer to the dominated absorbing mineral, or the position
600 is intermediate between expected B.C.I of the present phases, which are affecting the absorption
601 band (Fig. 7,8). Moreover, B.C. is not affected by grain size in almost mono-mineralic samples.
602 Differently, coarsening the grain size the B.C. of multi-mineral samples shifts from wavelengths
603 indicative of increasing Ca-px, or of the presence of ol or pl. Moreover, in VNIR reflectance
604 spectra of pl-rich rocks mafic minerals are less evident increasing the grain size.

605 B.D.I and II show a clearly linear relationship between co-genetically related rocks, so a trend of
606 spectral variation among different portion of a geological system can be regarded as the possible

607 expression of a mafic intrusive complex (Fig. 10,11). If bigger outcrops affect a pixel's spectral
608 information (here represented by slab spectra), we should expect a trend with lower B.D., indicated
609 by very low angle coefficient. Moreover where rock spectra (i.e. slab) are investigated, mafic
610 absorption will be clear only for abundances, at least, higher than 20% (Fig. 10). We have seen that
611 where spectra show a possible band saturation a linear trend is present with respect to a volumetric
612 variation on mineral composition (Fe^{2+}afu*%px in our case, Fig. 10c), maybe indicative of a
613 compositional variation on the magma chamber.

614 Further work will investigate the spectra applying a Gaussian modeling (e.g. MGM, Sunshine et al.,
615 1990, Clenet et al., 2013; EGO, Pompilio et al., 2009) to define and discuss the different absorption
616 processes that form composite bands.

617 **Acknowledgments**

618 The authors thanks Teresa Trua, Department of Earth Sciences, University of Parma, for the useful
619 discussions about rock petrography. Rock samples were kindly provided by Ottavia Zeda,
620 Department of Earth Sciences, University of Parma. Financial support by Agenzia Spaziale Italiana,
621 SIMBIO-SYS project. We also thanks L.C. Cheek and P. Pinet for their precious and pertinent
622 suggestions.

623 **References**

624 Bell, P.M. and Mao, H.K. (1973). Measurements of the polarized crystal field spectra of ferrous and
625 ferric iron in seven terrestrial plagioclases. Carnegie Institution of Washington Year Book, vol. 72,
626 574–576.

627 Boudreau, A.E. and McCallum, I.S. (1986). Investigations of the Stillwater Complex. Part III. The
628 Picket Pin Pt-Pd deposit. Economic Geology, 81, 1953-1975.

629 Boudreau, A.E. and McCallum, I.S. (1992). Concentration of Platinum Group Elements by
630 magmatic fluids in layered intrusions. Economic Geology, 87, 1830-1848.

631 Brown, S.M., and Elkins-Tanton, L.T. (2009). Compositions of Mercury's earliest crust from
632 magma ocean models. Earth Planetary Science Letters 286, 446-455.

633 Burns, R.G., (1970). Crystal field spectra and evidence for cation ordering in olivine minerals.
634 American Mineralogist, 55, 1608-1632.

635 Burns, R.G., (1993). Mineralogical applications of crystal field theory. Cambridge University Press,
636 Cambridge. 551 pp.

637 Campbell, I.H., and Murck, B.W. (1993). Petrology of the G and H chromitite zones in the
638 Mountain View area of the Stillwater Complex, Montana. Journal of Petrology, 34, 291-316.

639 Carli, C., and Sgavetti, M. (2011). Spectral characteristics of rocks: effects of composition and
640 texture and implications for the interpretation of planet surface compositions. Icarus, 211, 1034-
641 1048.

642 *Carli, C., Serventi, G., and Sgavetti, M. VNIR spectral characteristics of terrestrial igneous effusive*
643 *rocks: mineralogical composition and the influence of texture. Geological Society, London, Special*
644 *Publications, 401, in press.*

645 Cheek, L.C., Pieters, C.M., Boardman, J.W., Clark, R.N., Combe, J.P., Head, J.W., Isaacson, P.J.,
646 McCord, T.B., Moriarty, D., Nettles, J.W., Petro, N.E., Sunshine, J.M., and Taylor, L.A. (2011).
647 Goldschmidt crater and the Moon's north polar region: Results from the Moon Mineralogy Mapper
648 (M3). Journal of Geophysical Research,116, E00G02, doi:10.1029/2010JE003702.

649 Cheek, L. C., Pieters, C.M., Parman, S.W., Dyar, M.D., Speicher, E.A., and Cooper, R.F. (2011).
650 Spectral characteristics of PL with variable iron content: application to the remote sensing of the
651 lunar crust. Proceeding of 42° Lunar and Planetary Science Conference. Abs.#1617.

652 Clark, R.N., and Roush, T.L. (1984). Reflectance Spectroscopy: Quantitative Analysis Techniques
653 for Remote Sensing Applications. Journal of Geophysical Research, 89, 6329-6340.

654 Clenet, H., Pinet, P., Daydou, Y., Heuripeu, F., Rosemberg, C., Baratoux, D., Chevrel, S. (2011). A
655 new systematic approach using the Modified Gaussians Model: Insight for the characterization of
656 chemical composition of olivines, pyroxenes and olivine-pyroxene mixtures. Icarus, 213, 404-422.
657 Doi:10.1016/j.icarus.2011.03.002.

658 Clenet, H., Pinet, P., Ceuleneer, G., Daydou, Y., Heuripeu, F., Rosemberg, C., Birbring, J.-P.,
659 Bellucci, G., Altieri, F., and Gondet, B. (2013), A systematic mapping procedure based on the

Modified Gaussian Model to characterize magmatic units from olivine/pyroxenes mixtures: Application to the Syrtis Major volcanic shield on Mars. Journal of Geophysical Research, 118, 1632-1655, doi:10.1002/jgre.20112.

Cloutis, E.A., and Gaffey, M.J. (1991). Pyroxene spectroscopy revisited: spectral-compositional correlations and relationships to geothermometry, Journal of Geophysical Research, 96, 22,809-22,826.

Cloutis, E.A., Gaffey, M.J., Jackowski, T.L., and Reed, K.L. (1986). Calibrations of Phase Abundance, Composition, and Particle Size Distribution of Olivine-Orthopyroxene mixtures from Reflectance Spectra. Journal of Geophysical Research, 91, 11641-11653.

Donaldson Hanna, K., Cheek, L., Pieters, C., Mustard, J., Greenhagen, B., Thomas, I., and Bowles, N., Global Assessment of Pure Crystalline Plagioclase across the Moon and Implications for Evolution of the Primary Crust, Journal of Geophysical Research - Planets, in review

Elardo, S.M., Draper, D.S., and Shearer Jr., C.K.. (2011). Lunar Magma Ocean Crystallization revisited: Bulk composition, early cumulate mineralogy, and the source regions of the highlands Mg-suite. Geochimica et Cosmochimica Acta, 75, 3024-3045. doi:10.1016/j.gca.2011.02.033.

Ferrari, M.C., Sgavetti, M., and Chari, R. (1996). Multi-spectral facies in prevalent carbonate strata of an area of Migiurtinia (northen Somalia): analysis and interpretation. International Journal of Remote Sensing, 17, 111-130.

Harloff, J., and Arnold, G. (2001). Near-infrared reflectance spectroscopy of bulk analog materials for planetary crust. Planetary Space Science, 49 (2), 191-211.

Haskin, L.A. and Salpas, P.A. (1992). Genesis of compositional characteristics of Stillwater AN-I and AN-II thick anorthosite units. Geochimica et Cosmochimica Acta, 56, 1187-1212.

Herbert, F., Drake, M.J.,, Sonett, C.P. and Wiskerchen, M.J. (1977). Thermal history of lunar magma ocean. U.S. NASA Technical Memorandum 3511-31-33.

Shearer, C.K., Hess, P.C., Wieczorek, M.A., Pritchard, M.E., Parmentier, E.M., Borg, L.E., Longhi, J., Elkins-Tanton, L.T., Neal, C.R., Antonenko, I., Canup, R.M., Halliday, A.N., Grove, T.L., Hager, B.H., Lee, D-C. and Wiechert, U. (2006). Chapter 4: Thermal and Magmatic Evolution of the Moon. In: Ross, J.J. (Ed.), New Views of the Moon. Reviews in Mineralogy and Geochemistry 60. Virginia, 365-518.

Irvine, T.N., Keith, D.W., and Todd, S.G. (1983). The J-M platinum palladium reef of the Stillwater Complex, Montana: II. Origin by double-diffusive convective magma mixing and implications for the Bushveld Complex. Economic Geology, 78, 1287-1334.

Klima, R.L., Pieters, C.M., and Dyar, M.D. (2007). Spectroscopy of synthetic Mg-Fe pyroxenes I: Spinallowed and spin-forbidden crystal field bands in the visible and near-infrared. Meteoritics & Planetary Science 42, 235-253.

Klima, R.L., Dyar, M.D. and Pieters, C.M. (2011). Near-infrared spectra of clinopyroxenes: Effects of calcium content and crystal structure. Meteoritics & Planetary Science, 46, 379–395.

Kramer, G.Y., Kring, D.A., Nahm, A.L., and Pieters, C.M. (2013). Spectral and photogeologic mapping of Schrodinger Basin and implications for post-South Pole-Aitken impact deep subsurface stratigraphy. Icarus, 223, 131-148. doi:10.1016/j.icarus.2012.11.008.

Le Bas, M.J., Le Maitre, R.W., Streckeisen, A., and Zanettin, B. (1986). A chemical classification of volcanic rocks based on the total alkali-silica diagram. Journal of Petrology 27, 745-750.

Le Maitre, R.W., Streickeisen, A., Zanettin, B., LeBas, M.J., Bonin, B., Bateman, P., Bellieni, G., Dudek, A., Efremova, S., Keller, J., Lameyre, J., Sabine, P.A., Schmid, R., Sorensen, H., and Woolley, A.R. (2002). Igneous Rocks - A Classification and Glossary of Terms. Cambridge University Press, Cambridge, pp. 236.

Longhi, I., Sgavetti, M., Chari, R., and Mazzoli, C. (2001). Spectral analysis and classification of metamorphic rocks from laboratory reflectance spectra in the 0.4-2.5 μm interval: a tool for hyperspectral data interpretation. International Journal of Remote Sensing, 22, 3763-3782.

Longhi, J., and Ashwal, L.D. (1985). Two stages models for lunar and terrestrial anorthosites: Petrogenesis without a magma ocean. Proceeding of 15° Lunar Planetary Science Conference C571-C584.

Lucey, P., Korotev, R.L., Gillis, J.J., Taylor, L.A., Lawrence, D., Campbell, B.A., Elphic, R., Feldman, B., Hood, L.L., Hunten, D., Mendillo, M., Nobl, S., Papike, J.J., Reedy, R.C., Lawson, S., Prettyman, T., Gasnault, O., and Maurice, S. (2006). Chapter 2: Understanding the Lunar surface and Space-Moon interactions. In: Ross, J.J. (Ed.), New Views of the Moon. Reviews in Mineralogy and Geochemistry 60. Virginia, 83-219.

Matsunaga, T., Ohtake, M., Haruyama, J., Ogawa, Y., Nakamura, R., Yokota, Y., Morota, T., Honda, C., Torii, M., Abe, M., Nimura, T., Hiroi, T., Arai, T., Saiki, K., Takeda, H., Hirata, N.,

719 Kodama, S., Sugihara, T., Demura, H., Asada, N., Terazono, J., Otake, H. (2008). Discoveries on
720 the lithology of lunar crater central peaks by SELENE Spectral Profiler. Geophysical Research
721 Letters, 35, L23201, doi:10.1029/2008GL035868.

722 McCallum, I.S., Raedeke, L.D., and Mathez, E.A. (1980). Investigations in the Stillwater Complex:
723 Part I. Stratigraphy and structure of the Banded zone. American Journal of Science, 280A, 59-87.

724 McCallum, I.S. (1996). The Stillwater Complex. In: Cawthorn, R.G. (Eds.), Layered Intrusions.
725 Elsevier Science B.V. Press, Amsterdam, Nd, pp. 441-484.

726 McKay, D.S., Fruland, R.M. and Heiken, G.H. (1974). Grain size and evolution of lunar soils.
727 Proceedings of the fifth lunar conference, 1, 887-906.

728 Meurer, W.P. and Boudreau, A.E. (1995). The petrology and mineral compositions of the Middle
729 Banded series of the Stillwater Complex, Montana. Journal of Petrology, 37, 583-607.

730 Ohtake, M., Matsunaga, T., Haruyama, J., Yokota, Y., Morota, T., Honda, C., Ogawa, Y., Torii, M.,
731 Miyamoto, H., Arai, T., Hirata, N., Iwasaki, A., Nakamura, R., Hiroi, T., Sugihara, T., Takeda, H.,
732 Otake, H., Pieters, C.M., Saiki, K., Kitazato, K., Abe, M., Asada, N., Demura, H., Yamaguchi, Y.,
733 Sasaki, S., Kodama, S., Terazono, J., Shirao, M., Yamaji, A., Minami, S., Akiyama, H., and Josset,
734 J. (2009). The global distribution of pure anorthosite on the Moon. Nature 461,
735 doi:10.1038/nature08317.

736 Page, N. J. (1979). Stillwater Complex, Montana: Structure, mineralogy, and petrology of the Basal
737 Zone with emphasis on the occurrence of sulfides. U.S.G.S. Professional Paper 1038, 69p.

738 Page, N.J., and Moring, B.C. (1987). Petrology of the noritic and gabbronoritic rocks below the J-M
739 reef in the Mountain View area, Stillwater Complex, Montana. U.S.G.S. Bulletin, 1674-C, 1-47.

740 Pieters, C.M., Besse, S., Boardman, J., Buratti, B., Cheek, L., Clark, R.N., Combe, J.P., Dhingra,
741 D., Goswami, J.N., Green, R.O., Head, J.W., Isaacson, P., Klima, R., Kramer, G., Lundeen, S.,
742 Malaret, E., McCord, T., Mustard, J., Nettles, J., Petro, N., Runyon, C., Staid, M., Sunshine, J.,
743 Taylor, L.A., Thaisen, K., Tompkins, S., and Whitten, J. (2011). Mg-spinel lithology: A new rock
744 type on the lunar farside. Journal of Geophysical Research, 116, doi:10.1029/2010JE003727.

745 Pompilio, L., Pedrazzi, G., Sgavetti, M., Cloutis, E.A., Craig, M.A., and Roush, T.L. (2009).
746 Exponential Gaussian approach for spectral modeling: The EGO algorithm I. Band saturation.
747 Icarus 201 (2), 781-794.

Pompilio, L., Sgavetti, M., and Pedrazzi, G. (2007). Visible and near-infrared reflectance spectroscopy of pyroxene-bearing rocks: New constraints for understanding planetary surface compositions. Journal of Geophysical Research 112, E01004. doi:10.1029/2006JE002737.

Raedeke, L.D. and McCallum, I.S. (1980). A comparison of fractionation trends in the lunar crust and the Stillwater Complex. Proceeding of Lunar Highlands Crust Conference, 133-153.

Raedeke, L.D. and McCallum, I.S. (1984). Investigations of the Stillwater Complex: Part II. Petrology and petrogenesis of the Ultramafic series. Journal of Petrology, 25, 395-420.

Raedeke, L.D. (1982). Petrogenesis of the Stillwater Complex. Ph.D. thesis. University of Washington, 212p.

Serventi, G., Carli, C., Sgavetti, M., Ciarniello, M., Capaccioni, F., and Pedrazzi, G. (2013). Spectral variability of plagioclase-mafic mixtures 1): effects of chemistry and modal abundance in reflectance spectra of rocks and mineral mixtures, Icarus 226, 282-298, 10.1016/j.icarus.2013.05.041.

Smith, J.V., Anderson, A.T., Newton, R.C., Olsen, E.J., Wyllie, P.J., Crewe, A.V., Isaacson, M.S., Johnson, D. (1970). Petrology history of the Moon inferred from petrography, mineralogy, and petrogenesis of Apollo 11 rocks. In: Proceeding of the Apollo 11 Lunar Science Conference. Pergamon Press, 897-925.

Snyder, G.A., Taylor, L.A., and Neall, C.R. (1992). A chemical model for generating the sources of mare basalts: Combined equilibrium and fractional crystallization of the lunar magmasphere. Geochimica et Cosmochimica Acta, 56, 3809-3823.

Sunshine, J.M., and Pieters, C.M. (1991). Identification of modal abundances in the spectra of natural and laboratory pyroxene mixtures: A key component for remote analysis of lunar basalts. Proceeding of 22° Lunar Planetary Science Conference, 1361-1362.

Sunshine, J.M., Pieters, C.M., and Pratt, S.F. (1990). Deconvolution of mineral absorption bands: an improved approach. Journal of Geophysical Research, 95, 6955-6966.

Streckeisen, A. (1976). To each plutonic rock its proper name. Earth Science Review 12, 1-33.

Walker, D. (1983). Lunar and terrestrial crust formation. Proceedings 14° Lunar Planetary Science Conference, B17-B25.

776 Warren, P.H. (1985). The magma ocean concept and lunar evolution. Annual Review of Earth
777 Planetary Science, 13, 201-240.

778 Wood, J.A., Dickey, J.S., Marvin, U.B., and Powell, B.N. (1970). Lunar anorthosites and a
779 geophysical model of the Moon. In: Proceeding of the Apollo 11 Lunar Science Conference.
780 Pergamon Press,, 965-988.

781 Yamamoto, S., Nakamura, R. Matsunaga, T. Ogawa, Y., Ishihara, Y., Morota, T., Hirata, N.,
782 Ohtake, M., Hiroi, T., Yokota, Y., and Haruyama, J. (2012). Massive layer of pure anorthosite on
783 the Moon. Geophysical Research Letters, 39, 10.1029/2012GL052098.

784 **Figure's Captions:**

785 Figure 1 – a) Mg# of opx vs. An# of pl, distribution of Series and Zones, modified after McCallum
786 (1996). Samples studied in this paper are plotted (red and blue diamond). b) samples are distributed
787 vs. the stratigraphy of the igneous layering as defined by McCallum et al. (1980) and Radeke and
788 McCallum (1984). Samples StC2, StC4, StC7, StC8, StC12, StC13, StC14, StC16, StC17, StC20
789 and StC25 (italic) are positioning following the Mg# vs. An#, mineral chemistry, mineral
790 assemblages and petrographic characteristics. Other samples are placed in noted zone. In a): UmS,
791 Ultramafic Series; LBdS, MBdS, UBdS, Lower, Middle, Upper Banded Series; N, Norite Zone;
792 GN, Gabbronorite Zone; OB, olivine-bearing Zone.

793 Figure 2 – shows all the absorptions identified in our samples. C.F. absorption are listed as I, II, III,
794 IV, V; vibrational absorption are listed as 'a' (e.g. O-H-O), 'b' (e.g. OH-), 'c, d' (e.g. M-OH). See
795 text for more details.

796 Figure 3 – Gabbroic rocks diagram (after Streickeisen (1976)). The mineral abundances have been
797 estimated by point counter analysis of representative thin sections, the number of points varies with
798 the crystal sizes of each samples, but we counted from ca. 600 to 800 points for sample (see also
799 Table 1). a) all the samples are plotted, except the StC3 sample because it contains opaques >90%;
800 b) pl-px rocks are plotted. In both boxes the pl vertex shows anorthositic rocks, whereas in the
801 opposite side are present the ultramafic rocks.

802 Figure 4 – a) mafic mineral compositions are showed. Opx vary from En91 to En61 and cpx from
803 En48 to En39 (Wo ~45). Olivines vary from 88 to 76 Fo%. All minerals show an iron enrichment
804 from UmS to BdS. b) plagioclase diagram, An varies from 70 to 89, with UmS pl in general more
805 albitic than BdS pl. Multiple measurements are plotted for each samples in a) and b).

Wo=wollastonite%, Di=diopside%, Hd=Hedembergite%, En=Enstatite%, Fs=Ferrosilite%; Fo=Fosterite%; Or=Ortoclase%, Ab=Albite%, An=Anortite%

Figure 5 – Powder (<0.250 mm) spectra divided in four main groups considering different C.F. absorption, reflectance and spectral shape. a) pl rich rocks (Group 1a_p), higher reflectance spectra, dominated by band V; ; b) px rich samples, spectra dominated by band I and II (Group 2a_p), and spectra showing an association of Band I, V, II (Group 2b_p, samples StC10,13,14, grey lebel); c) ol bering rocks, two spectra show ol band I absorption (Group 3a_p), two spectra are almost featureless, low albedo (Group 3b_p), reflectance of StC17 is shifted of - 3%; d) chromite bearing rocks: Group 4a_p is dominate by chromite spectra, with a weak 1μm band which can be affected also by ol. Group 4b_p, px-chromite samples have clear band I, and band II spectrally affected by the chromite absortpion towards infrared. Reflectance of StC1 is shifted of + 5% for clarification. See text for more details.

Figure 6 – Slab spectra divided in four main groups considering different C.F. absorptions, reflectance and spectral shape. a) pl rich rocks, higher reflectance spectra dominated by band V (Group 1_s); b) px rich rocks, spectra dominated by band I and II; c) ol bearing rocks, spectra showing blue slope and a weak (Group 3a_s) or absent (Group 3b_s) band I, reflectance shift: StC5 +10%, StC16 +5%, StC19 -5%, for clarity; d) low albedo spectra with very low absoprtion contrast, chromite bearing samples (Group 4a_s). Group 4b_s show px-chromite samples, absorbing contrast and reflectance are lower than px-bearing sample in Group 2_s. Reflectance of StC6 is shifted of – 5% for clarification. See text for more details.

Figure 7 – B.C. I vs. pyroxenes composition, expressed as Fs. We have considered a weighted value due to the presence of both opx and cpx, to compare with Cloutis and Gaffey (1991), grey symbols. Grain sizes <0.050 mm and <0.125 mm were produced only for selected samples. a) powder (<0.050 mm) spectra, a color density bar is used to show the difference of Fs value for opx and cpx on samples with both pyroxenes. The color variation is indicative of the px abundances (dark blue end indicates the Fs% of the most abundant px, light end the Fs% of the less abundant px); b) powders <0.125 mm compare to a) plot; c) powders <0.250 compare to b) plot, more samples are studied, pl rich samples StC9 and StC11 are not plotted here (B.C.V at ~1.27 μm); d) Slab spectra compare to powder spectra, all samples are plotted, pl rich samples are dominated by band V position (>1.050 μm). The box in a,b,c indicate, from bottom to top, the groups 1, 2, 3 discussed in the spectral parameters section.

Figure 8 – B.C.I vs. pyroxene composition, expressed as weighted Wo%. Powder spectra show a B.C. closer to pyroxene of Cloutis and Gaffey (1991). Ol rich samples are out from the trend. See the text for more details.

Figure 9 – B.C.II plotted vs weighted Fs.% (a) and Wo% (b). The B.C. position is affected by the OH- vibrational band at 1.9μm. c) enlarged view of b) (grey dashed box) with wo < 20%; it shows the B.C.II for opx-rich samples with <250 μm size, for which we have the highest number of samples. The B.C.II moves towards higher wavelengths increasing Wo% content.

Figure 10 – B.D.I vs. pyroxene abundance (a, b), vs. total volumetric Fe^{2+} (Fe^{2+} afu (opx)*opx%+ Fe^{2+} afu (cpx)*cpx%; c,d). a) here are not considered the spectra of StC20, 25. b) all samples. Powder B.D.I is linearly related to the px abundance, whereas slab B.D.I shows low R^2. c) slabs B.D.I are linearly related with high R^2 vs. the volumetric iron. d) powder of spectra are not linearly related to the volumetri iron, the trend can be described with a second polynomial equation. See text for more details. In a) selected samples are labeled, in b) are labeled StC20,25. In c), d) samples are in the same order of a) from left to right, with StC20,25 that have the two highest total volumetric iron values.

Figure 11 – B.D.II of powders are linearly related to the px abundance. a) selected samples, b) all samples (see also Fig. 10a,b).

Figure 12 – pl-mafic abundance vs. FeOtot from XRF (see table 2). a) pl abundance decrease increasing the iron bulk in the samples, mafic mineralogy shows the opposite behavior. b) show as pl ferrous iron abundance (from EMPA, see table 3) varies from high abundance for pl-rich rocks to low Fe^{2+} abundance for pl-poor samples.

Figure 13 – The stratigraphy of the igneous layering (e.g. defined by McCallum et al. (1980) and Radeke and McCallum (1984)) vs. the spectral stratigraphy from the spectral groups for both powder and slab. The Groups 1 and 2 divided the stratigraphy in two bigger layers for slab spectra. Whereas for powder: Group 1 is characterized by samples from the Anorthosite I and II Zone, and Ol-bearing Zone is covered by Group 2b_p and Group 3b_p. Group 4 and Group 3a samples are from Peridotite Zone. '?' indicates the UBdS where we have one samples with very high ol alteration, not representative of original mineralogy.

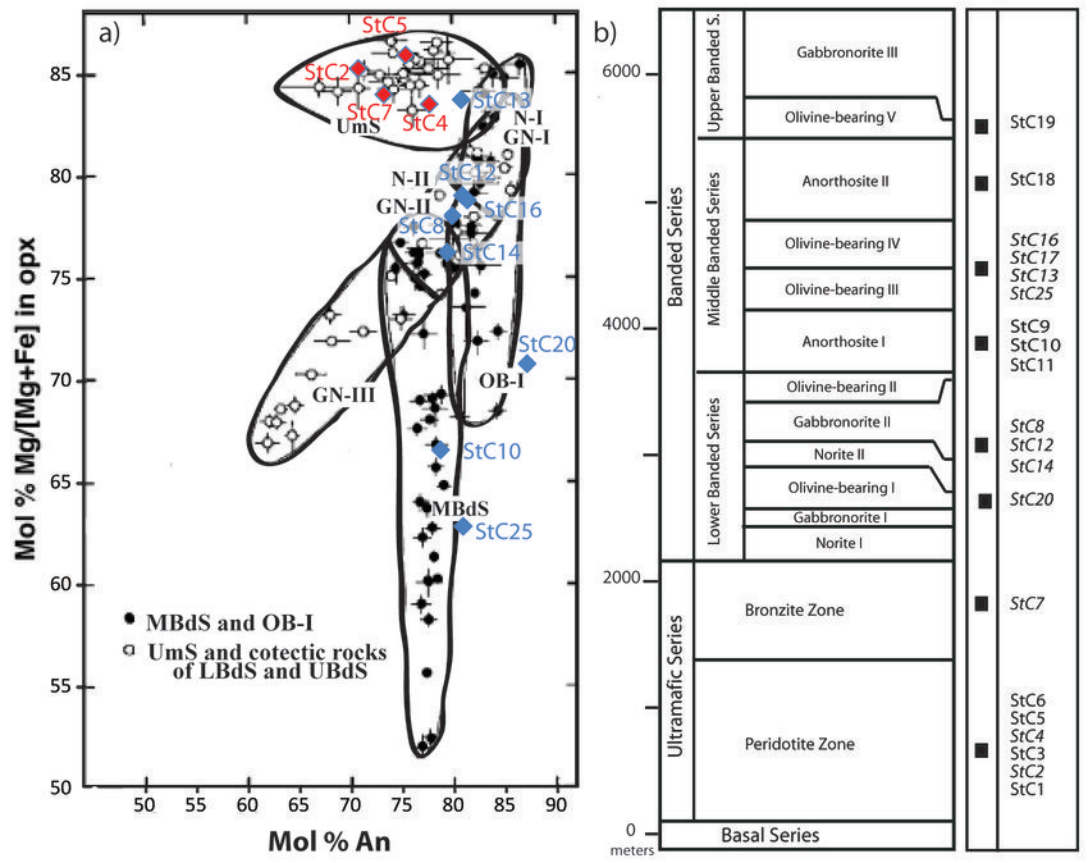
a)
StC5
StC2
StC7
StC4
StC13
UmS
N-I
GN-I
N-II
StC12
GN-II
StC16
StC8
StC14
StC20
OB-I
GN-III
StC10
MBdS
StC25
MBdS and OB-I
UmS and cotectic rocks of LBdS and UBdS
Mol % Mg/[Mg+Fe] in opx
Mol % An
50
55
60
65
70
75
80
85
90
b)
6000
4000
2000
0
meters
Banded Series
Upper Banded S.
Middle Banded Series
Lower Banded Series
Ultramafic Series
Gabbronorite III
Olivine-bearing V
Anorthosite II
Olivine-bearing IV
Olivine-bearing III
Anorthosite I
Olivine-bearing II
Gabbronorite II
Norite II
Olivine-bearing I
Gabbronorite I
Norite I
Bronzite Zone
Peridotite Zone
Basal Series
StC19
StC18
StC16
StC17
StC13
StC25
StC9
StC10
StC11
StC8
StC12
StC14
StC20
StC7
StC6
StC5
StC4
StC3
StC2
StC1

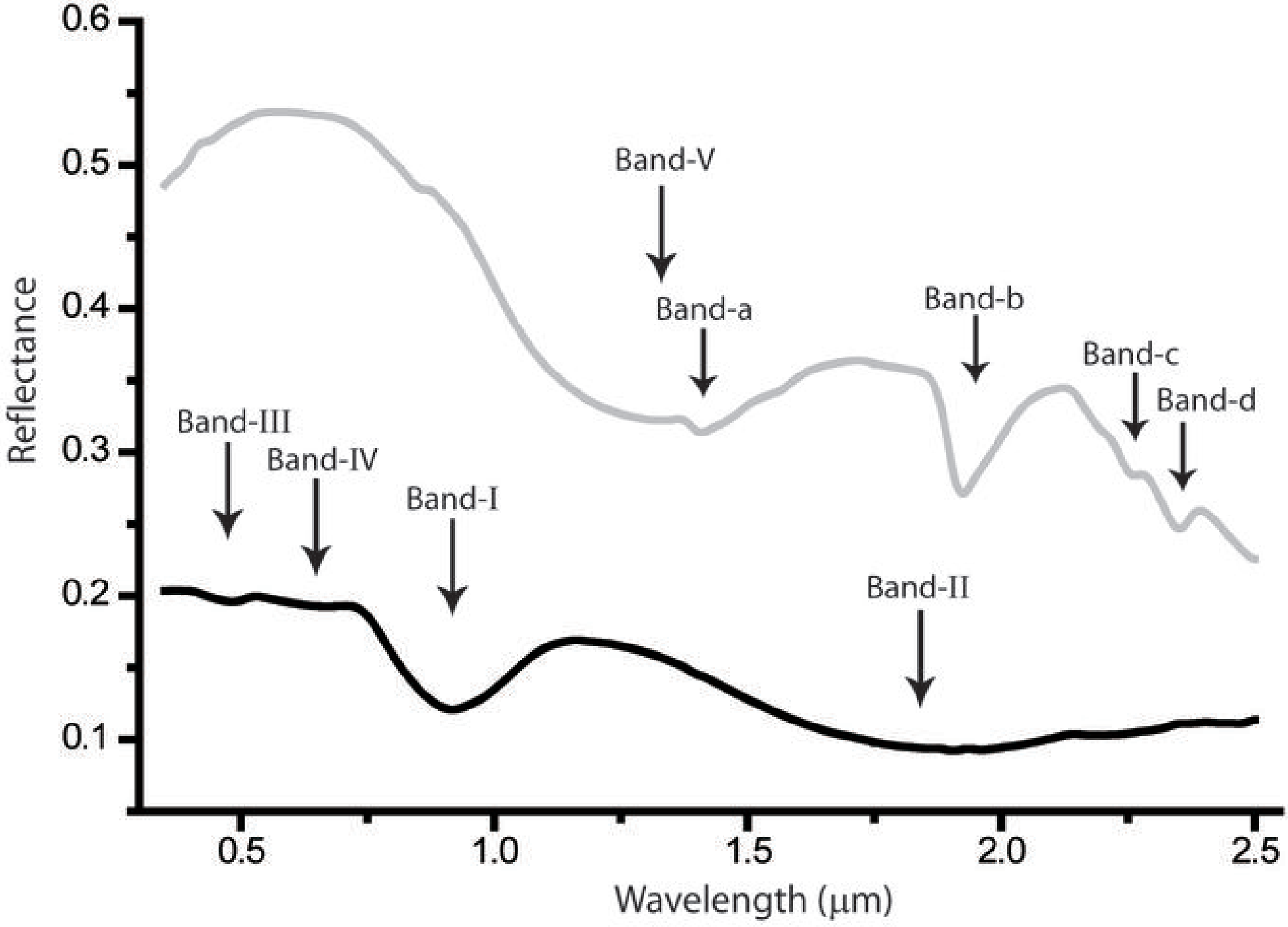
0.6
0.5
0.4
0.3
0.2
0.1
Reflectance
Band-V
Band-a
Band-b
Band-c
Band-d
Band-III
Band-IV
Band-I
Band-II
0.5
1.0
1.5
2.0
2.5
Wavelength (μm)

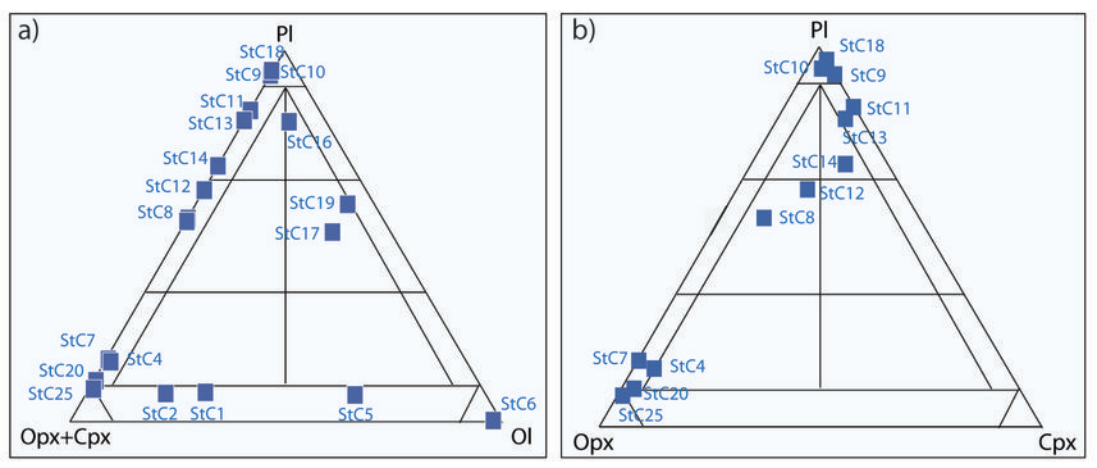
a)
Pl
StC18
StC9
StC10
StC11
StC13
StC16
StC14
StC12
StC8
StC19
StC17
StC7
StC4
StC20
StC25
StC2
StC1
StC5
StC6
Opx+Cpx
Ol
b)
Pl
StC18
StC10
StC9
StC11
StC13
StC14
StC12
StC8
StC7
StC4
StC20
StC25
Opx
Cpx

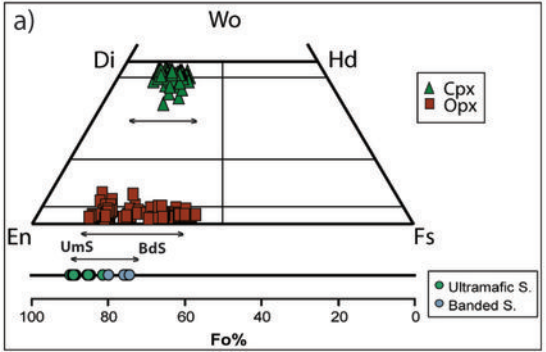
a)
Wo
Di
Hd
Cpx
Opx
En
Fs
UmS
BdS
Ultramafic S.
Banded S.
100
80
60
40
20
0
Fo%

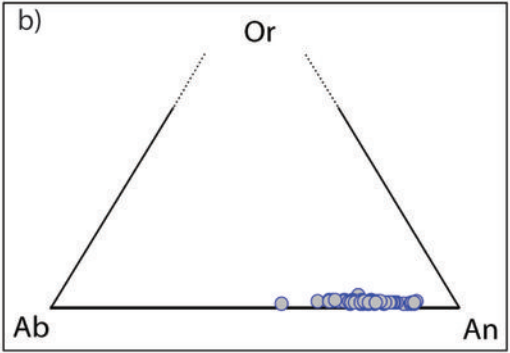
b)
Or
Ab
An

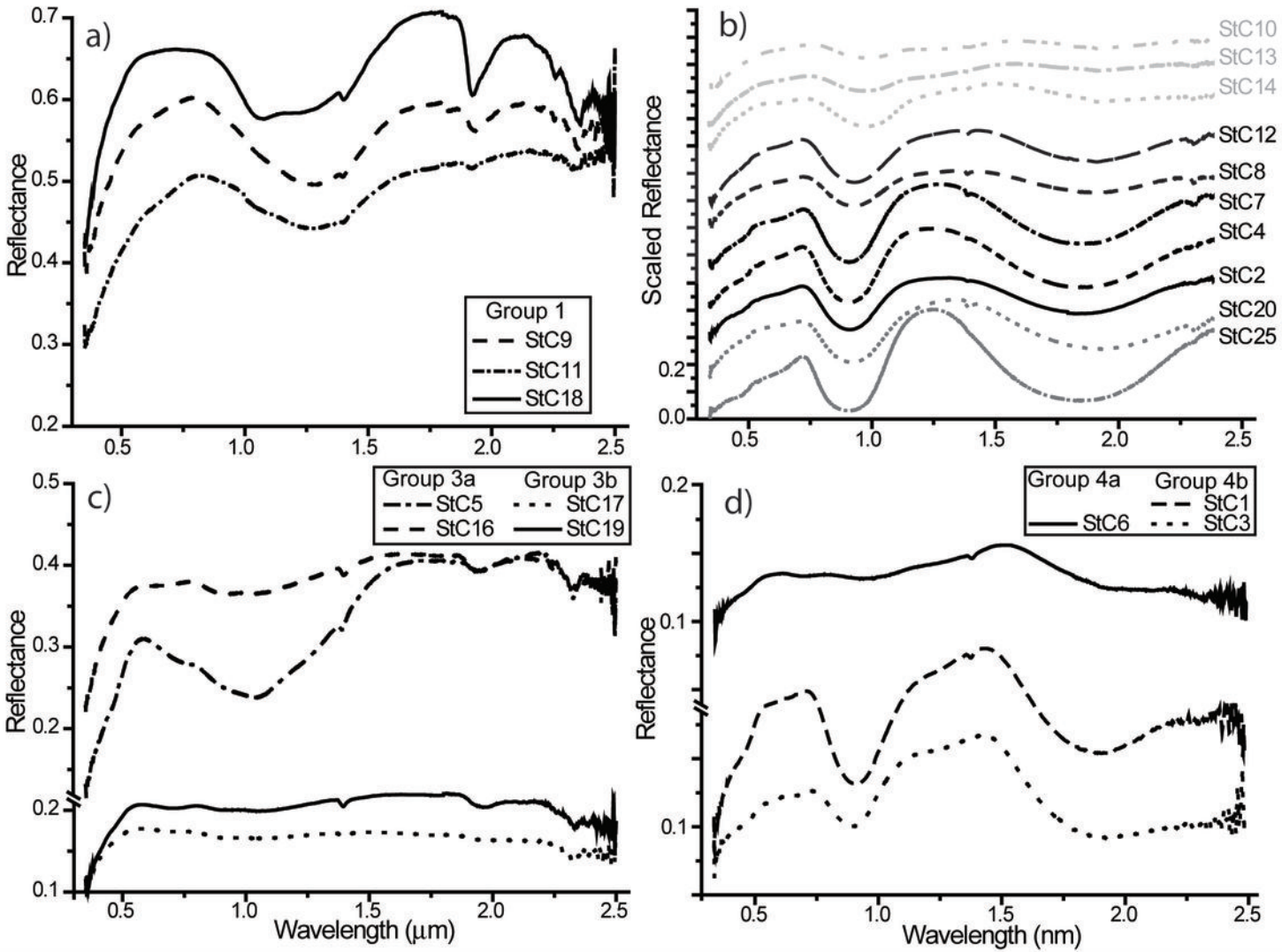
a)
Reflectance
Group 1
StC9
StC11
StC18
b)
Scaled Reflectance
StC10
StC13
StC14
StC12
StC8
StC7
StC4
StC2
StC20
StC25
c)
Group 3a
Group 3b
StC5
StC17
StC16
StC19
Reflectance
Wavelength (μm)
d)
Group 4a
Group 4b
StC1
StC6
StC3
Reflectance
Wavelength (nm)

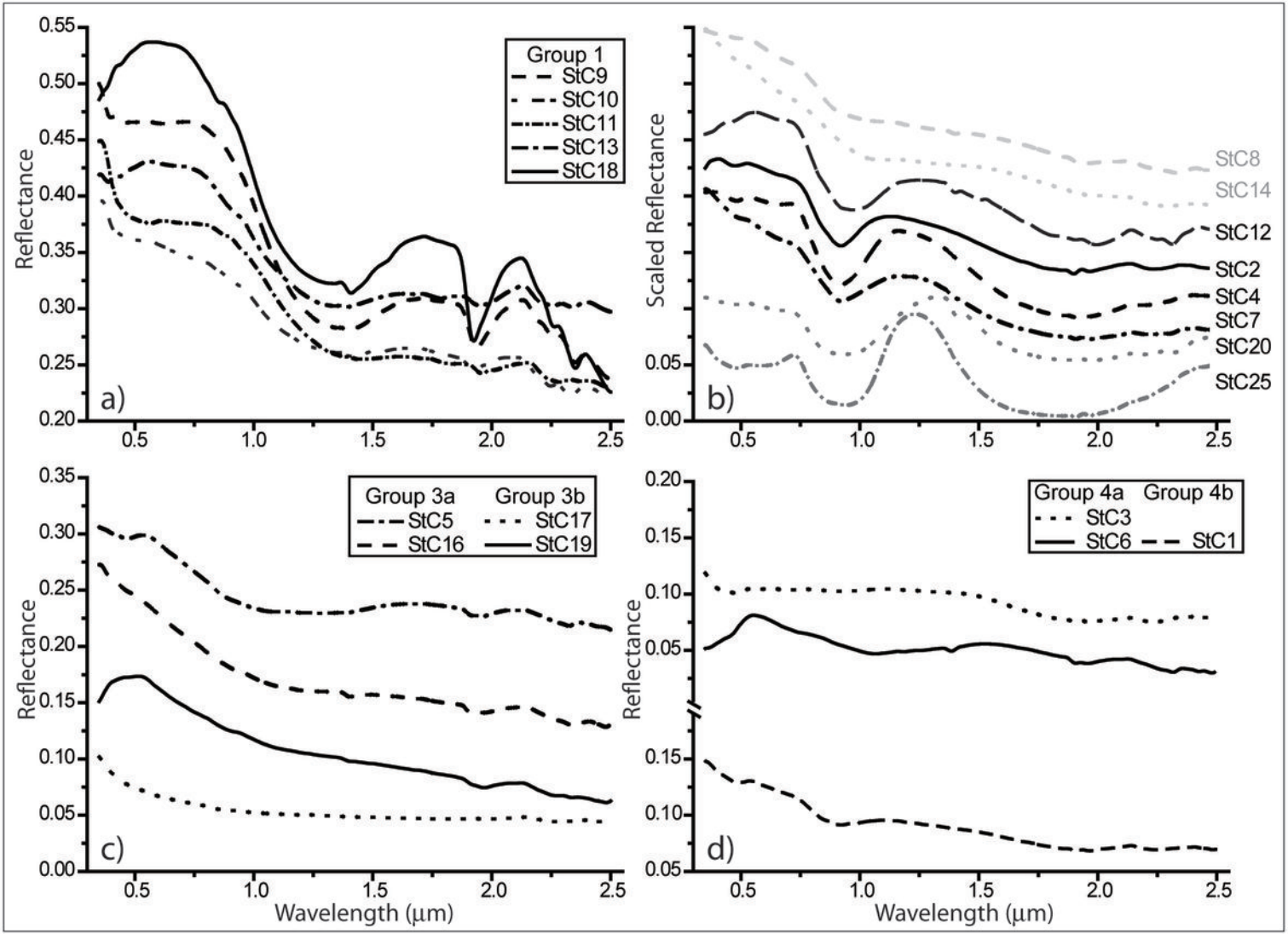
Group 1
StC9
StC10
StC11
StC13
StC18
Reflectance
a)
Scaled Reflectance
StC8
StC14
StC12
StC2
StC4
StC7
StC20
StC25
b)
Group 3a
Group 3b
StC5
StC17
StC16
StC19
Reflectance
c)
Wavelength (μm)
Group 4a
Group 4b
StC3
StC6
StC1
Reflectance
d)
Wavelength (μm)

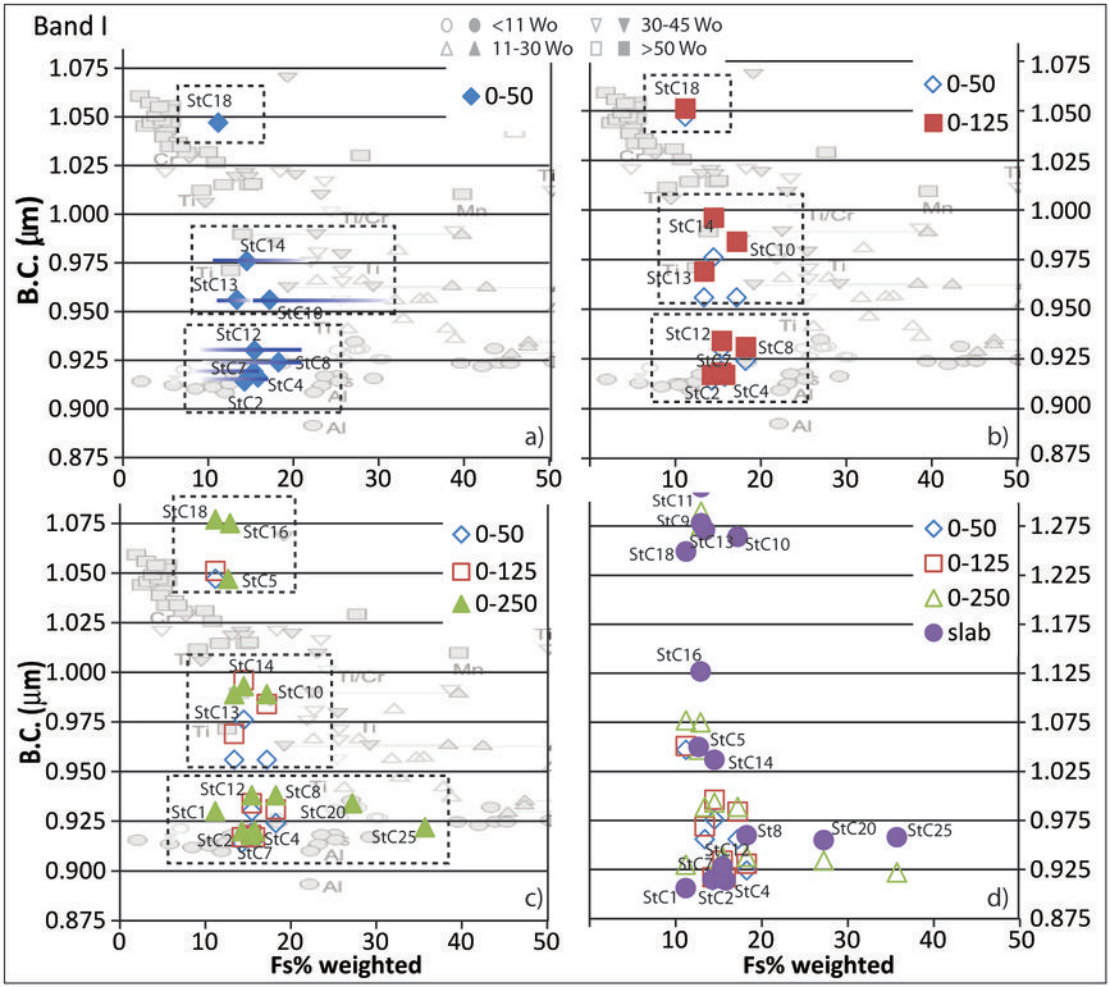
Band I
<11 Wo
11-30 Wo
30-45 Wo
>50 Wo
B.C. (µm)
Fs% weighted
a)
b)
c)
d)
0-50
0-125
0-250
slab
StC18
StC14
StC13
StC10
StC12
StC8
StC7
StC4
StC2
StC5
StC16
StC1
StC20
StC25
StC11
StC9
StC3
Ti
Ti/Cr
Mn
Al

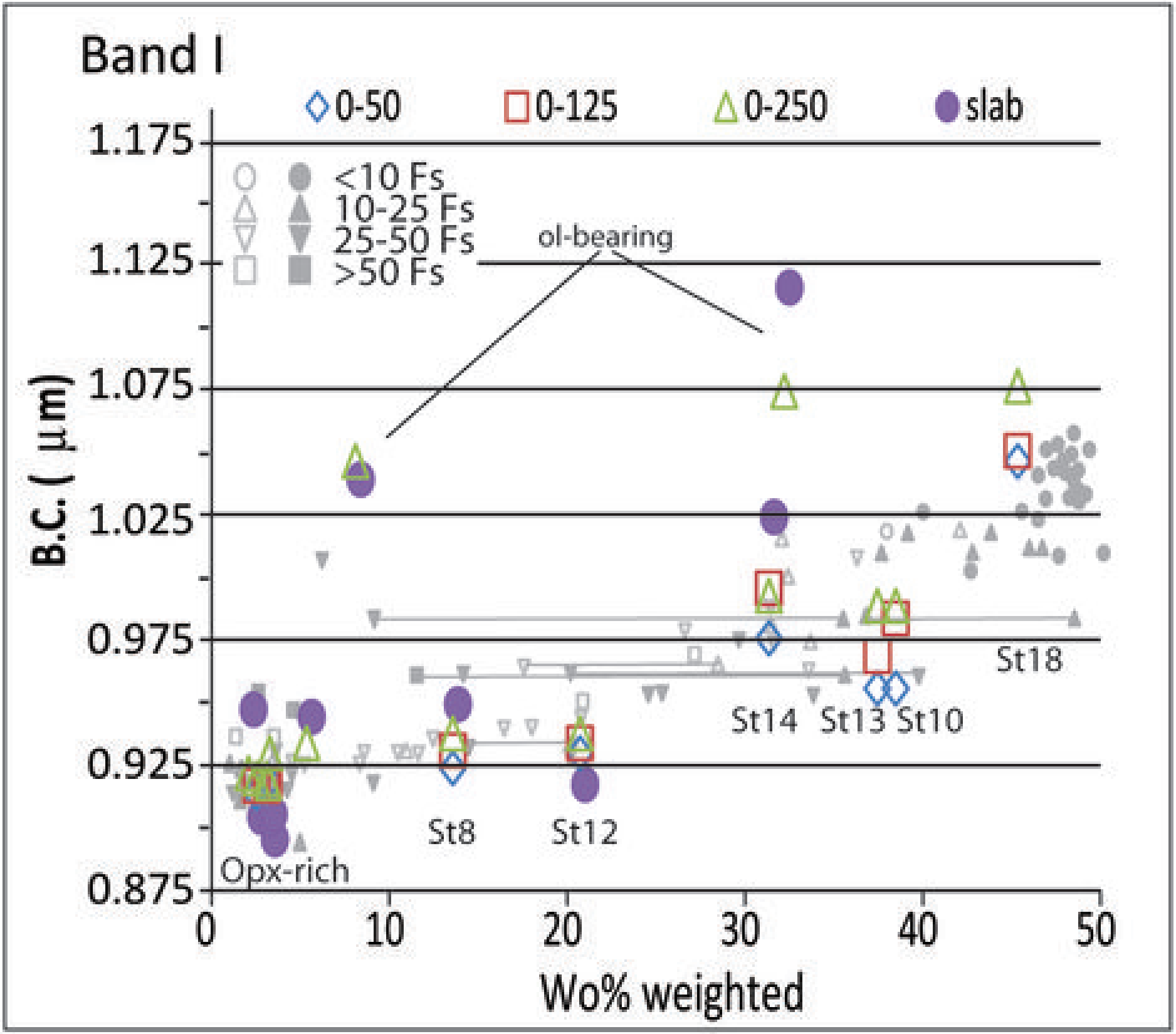
Band I
0-50
0-125
0-250
slab
<10 Fs
10-25 Fs
25-50 Fs
>50 Fs
ol-bearing
1.175
1.125
1.075
1.025
0.975
0.925
0.875
B.C. (μm)
St18
St14
St13
St10
St8
St12
Opx-rich
0
10
20
30
40
50
Wo% weighted

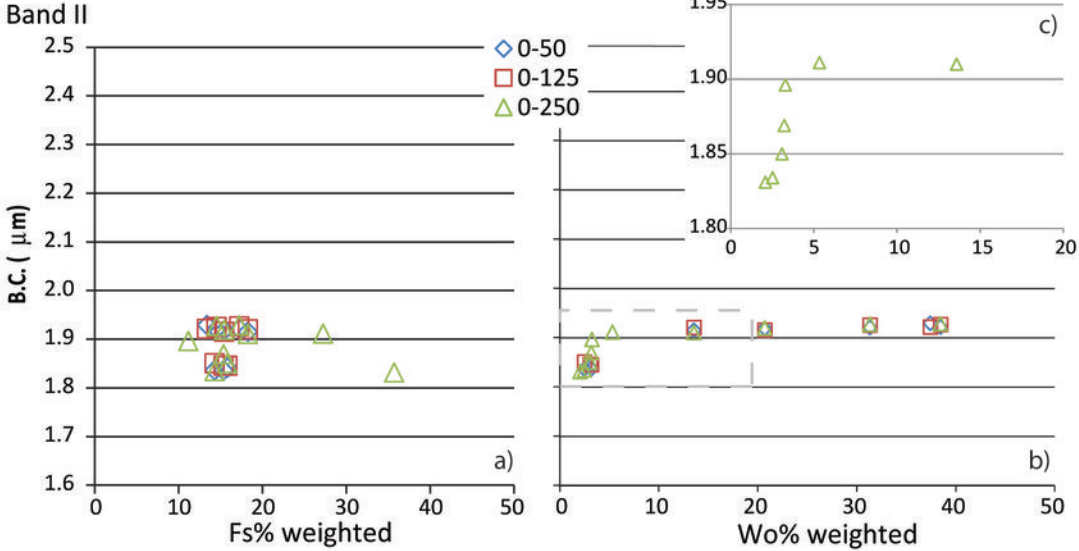
Band II
0-50
0-125
0-250
B.C. (µm)
2.5
2.4
2.3
2.2
2.1
2.0
1.9
1.8
1.7
1.6
0
10
20
30
40
50
Fs% weighted
a)
Wo% weighted
b)
c)
1.95
1.90
1.85
1.80
0
5
10
15
20

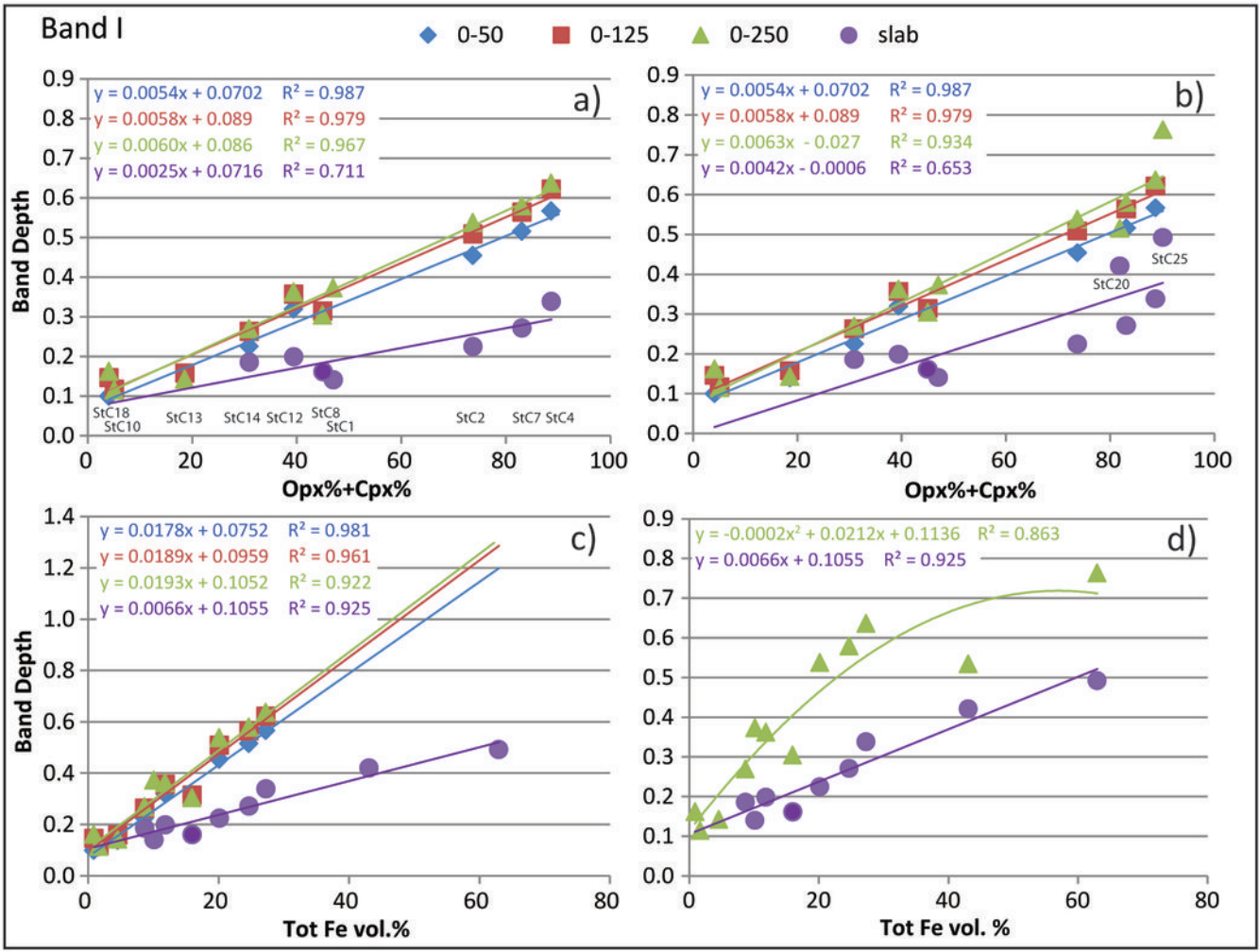
Band I
0-50
0-125
0-250
slab
a)
y = 0.0054x + 0.0702 R² = 0.987
y = 0.0058x + 0.089 R² = 0.979
y = 0.0060x + 0.086 R² = 0.967
y = 0.0025x + 0.0716 R² = 0.711
Band Depth
Opx%+Cpx%
StC18
StC10
StC13
StC14
StC12
StC8
StC1
StC2
StC7
StC4
b)
y = 0.0054x + 0.0702 R² = 0.987
y = 0.0058x + 0.089 R² = 0.979
y = 0.0063x - 0.027 R² = 0.934
y = 0.0042x - 0.0006 R² = 0.653
StC25
StC20
Opx%+Cpx%
c)
y = 0.0178x + 0.0752 R² = 0.981
y = 0.0189x + 0.0959 R² = 0.961
y = 0.0193x + 0.1052 R² = 0.922
y = 0.0066x + 0.1055 R² = 0.925
Band Depth
Tot Fe vol.%
d)
y = -0.0002x² + 0.0212x + 0.1136 R² = 0.863
y = 0.0066x + 0.1055 R² = 0.925
Tot Fe vol. %

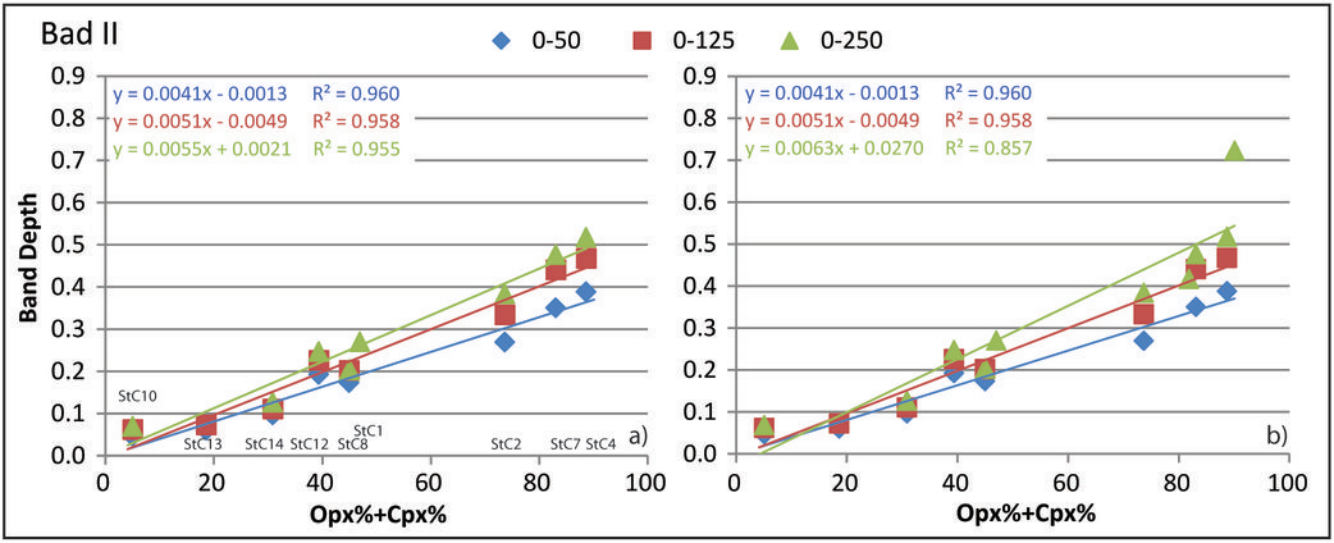
Bad II
0-50
0-125
0-250
y = 0.0041x - 0.0013 R² = 0.960
y = 0.0051x - 0.0049 R² = 0.958
y = 0.0055x + 0.0021 R² = 0.955
Band Depth
Opx%+Cpx%
StC10
StC13
StC14
StC12
StC8
StC1
StC2
StC7
StC4
a)
y = 0.0041x - 0.0013 R² = 0.960
y = 0.0051x - 0.0049 R² = 0.958
y = 0.0063x + 0.0270 R² = 0.857
Opx%+Cpx%
b)

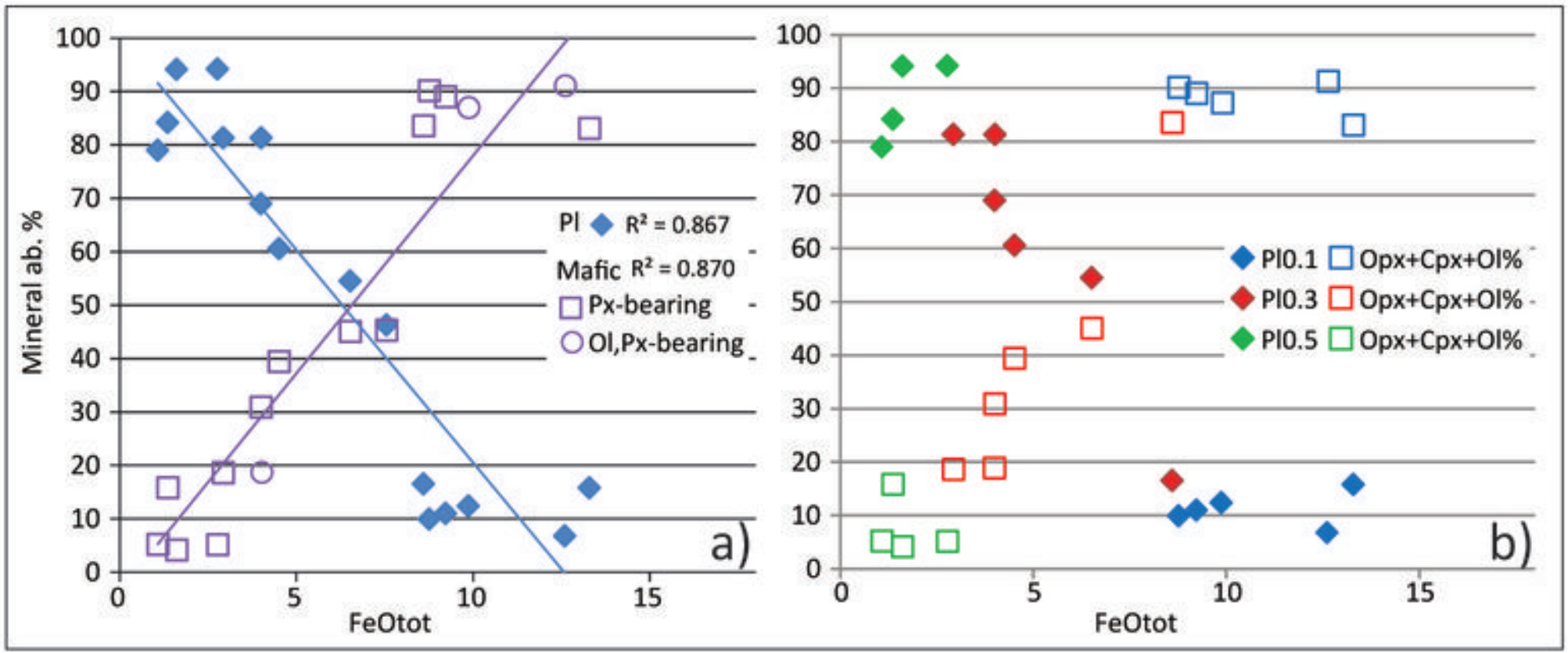
Mineral ab. %
FeOtot
Pl R² = 0.867
Mafic R² = 0.870
Px-bearing
Ol,Px-bearing
a)
Pl0.1 Opx+Cpx+Ol%
Pl0.3 Opx+Cpx+Ol%
Pl0.5 Opx+Cpx+Ol%
b)

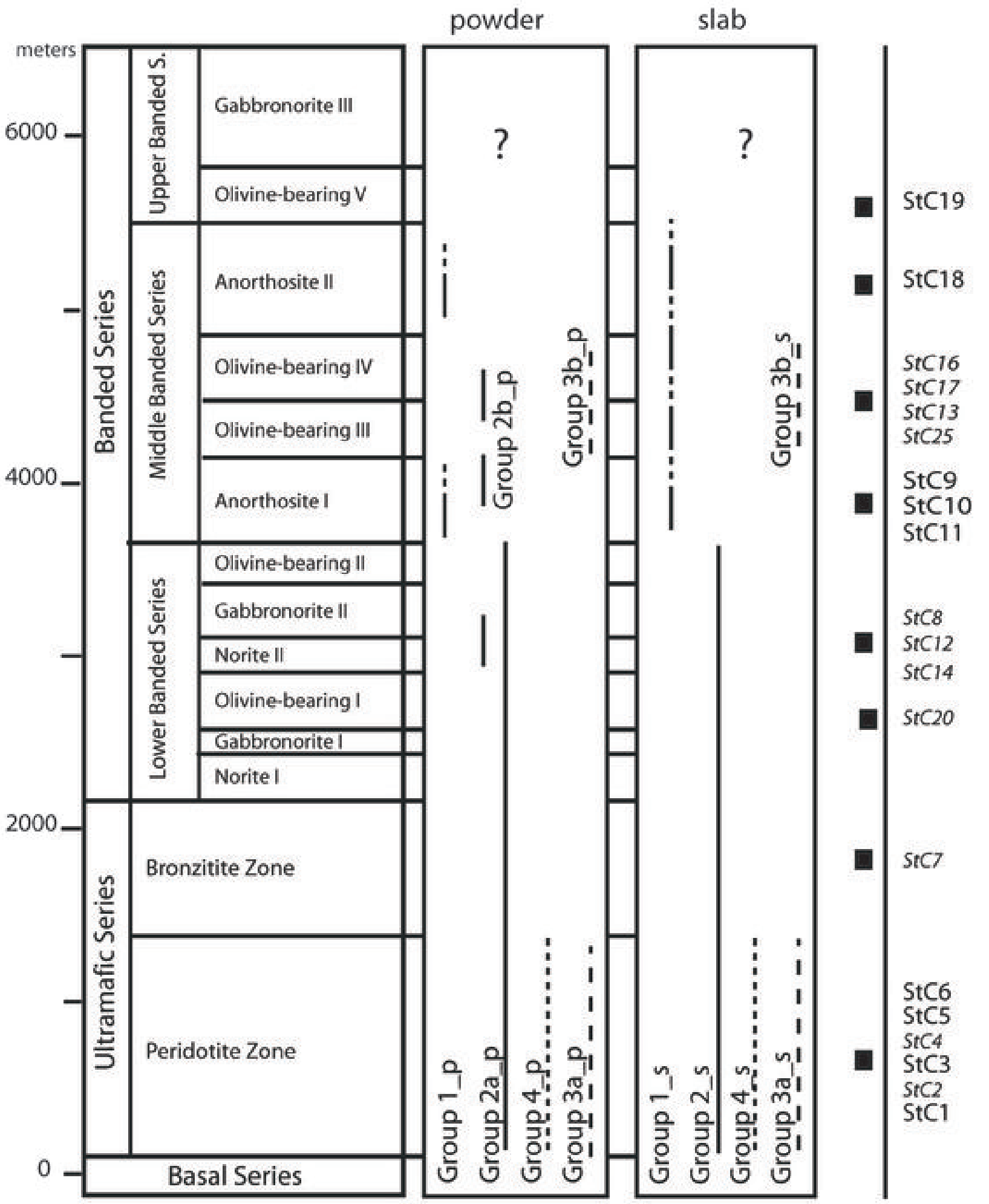
powder
slab
meters
6000
4000
2000
0
Banded Series
Upper Banded S.
Middle Banded Series
Lower Banded Series
Ultramafic Series
Gabbronorite III
Olivine-bearing V
Anorthosite II
Olivine-bearing IV
Olivine-bearing III
Anorthosite I
Olivine-bearing II
Gabbronorite II
Norite II
Olivine-bearing I
Gabbronorite I
Norite I
Bronzitite Zone
Peridotite Zone
Basal Series
?
?
Group 1_p
Group 2a_p
Group 2b_p
Group 3a_p
Group 3b_p
Group 4_p
Group 1_s
Group 2_s
Group 3a_s
Group 3b_s
Group 4_s
StC19
StC18
StC16
StC17
StC13
StC25
StC9
StC10
StC11
StC8
StC12
StC14
StC20
StC7
StC6
StC5
StC4
StC3
StC2
StC1

Mineral abundance

sample	Pl	Cpx	Opx	Ol	Op	Zoisite	Alteration	n.° point
StC1	5.10	0.00	47.00	19.70	28.30	0.00	Rare	792
StC2	12.40	0.00	73.70	13.30	0.60	0.00	Rare	676
StC3					>90		Rare	601
StC4	11.00	2.80	85.90	0.30	0.00	0.00	Rare	775
StC5	6.80	3.10	25.70	62.30	2.00	0.00	Few	762
StC6	0.00	0.00	0.00	45.10	54.90	0.00	Rare	603
StC7	16.50	1.00	82.10	0.40	0.00	0.00	Rare	711
StC8	54.50	10.00	35.00	0.00	0.10	0.50	Rare	804
StC9	79.00	5.20	0.00	0.00	0.00	15.70	Pl	705
StC10	94.20	4.30	0.80	0.00	0.00	0.70	Rare	718
StC11	84.20	15.80	0.00	0.00	0.00	0.00	Rare	755
StC12	60.60	17.30	22.10	0.00	0.00	0.00	Rare	720
StC13	81.30	15.50	3.10	0.00	0.00	0.10	Rare	686
StC14	69.00	21.20	9.70	0.00	0.00	0.00	Rare	739
StC16	81.30	5.50	2.40	10.80	0.00	0.00	Few-Ol	779
StC17	46.30	7.30	3.70	34.30	0.00	8.40	Pl; Ol	630
StC18	94.10	4.10	0.00	0.00	0.00	1.80	Few-Pl	713
StC19	58.40	5.50	0.00	35.70	0.50	0.00	Ol	622
StC20	13.20	4.60	63.90	1.00	0.50	0.50	Rare	613
StC25	9.90	1.40	88.70	0.00	0.00	0.00	Rare	653

Table 1 – Stillwater Complex samples: minerals abundance from point counting under optical microscope. Op. indicates opaque minerals. Alteration col. indicates sample alteration. n.° poi indicates the total number of counted points.

XRF - bulk rock composition

	STC1	STC2	STC3	STC4	STC5	STC6	STC7	STC8	STC9	STC10	STC11	STC12	STC13	STC14	STC16	STC17	STC18	STC19	STC20	STC25
SiO_2	32.34	52.19	19.66	54.82	41.57	11.51	54.55	51.10	48.51	49.26	49.14	50.38	49.37	50.41	46.83	45.06	48.70	43.41	51.48	54.18
TiO_2	0.22	0.12	0.32	0.12	0.04	0.47	0.11	0.15	0.07	0.11	0.11	0.10	0.12	0.14	0.05	0.04	0.09	0.06	0.23	0.11
Al_2O_3	7.52	2.85	12.51	3.91	3.14	11.76	5.41	16.83	31.57	27.23	30.75	20.39	26.57	21.07	26.74	21.15	29.44	16.57	9.22	3.89
Fe_2O_{3tot}	16.48	10.80	19.71	10.15	13.77	29.52	9.34	7.06	1.18	3.03	1.49	4.95	3.22	4.45	4.36	8.09	1.79	11.15	14.30	9.63
MnO	0.17	0.18	0.17	0.19	0.17	0.16	0.18	0.13	0.02	0.05	0.02	0.10	0.06	0.09	0.06	0.10	0.03	0.14	0.22	0.17
MgO	27.86	31.03	20.07	27.33	38.56	18.22	25.69	12.40	0.84	3.29	1.04	9.61	3.76	7.71	6.73	13.77	2.05	18.12	16.58	27.36
CaO	1.63	2.79	1.18	3.35	1.85	0.43	4.45	10.70	16.13	15.79	15.76	13.15	15.55	15.46	13.68	10.84	15.92	8.90	6.27	3.45
Na_2O	0.10	0.23	0.06	0.26	0.25	0.03	0.42	1.11	2.17	1.86	2.21	1.33	1.84	1.48	1.78	1.25	2.25	0.94	0.37	0.31
K_2O	0.02	0.04	0.01	0.04	0.03	0.01	0.06	0.08	0.09	0.08	0.12	0.06	0.10	0.13	0.06	0.04	0.08	0.05	0.49	0.05
P_2O_5	0.01	0.01	0.00	0.01	0.01	0.01	0.01	0.01	0.01	0.01	0.02	0.01	0.01	0.01	0.01	0.01	0.01	0.01	0.01	0.01
Tot.	86.4	100.2	73.7	110.2	99.4	72.1	100.2	99.6	100.6	100.7	100.7	100.1	100.6	100.9	100.3	100.4	100.4	99.4	99.2	99.2
Cr (ppm)	113464	3149	195794	3167	5090	211616	3274	635	65	302	53	615	259	660	75	57	122	230	1476	3410
L.O.I.	*0.44*	*1.25*	*-0.40*	*0.79*	*4.55*	*0.37*	*1.20*	*1.23*	*0.70*	*0.54*	*0.68*	*0.83*	*0.59*	*0.92*	*2.67*	*5.16*	*1.60*	*7.75*	*1.90*	*0.76*
FeO	4.41	8.30	2.64	8.21	10.44	1.75	6.61	4.76	0.88	2.22	1.10	3.87	2.56	3.96	3.02	4.77	1.55	5.20	8.97	7.72
Fe_2O_3	11.58	1.58	16.78	1.03	2.17	27.58	2.00	1.77	0.20	0.56	0.27	0.65	0.38	0.05	1.00	2.79	0.07	5.37	4.33	1.05
Σ (FeO +Fe_2O_3)	15.99	9.88	19.42	9.24	12.61	29.33	8.61	6.53	1.08	2.78	1.37	4.52	2.94	4.01	4.02	7.56	1.62	10.57	13.30	8.77

Table 2 – Bulk rock chemistry from XRF measurements for major elements and chromium. We report the L.O.I. (loos on ignition) and the amount of ferrous and ferric iron from chemical analysis (Pratt and Wilson wet chemical methods).

orthopyroxene

	St1	St2	St3	St4	St5	St7	St8	St10	St12	St13	St14	St16	St20	St25
SiO2	57.14	56.90	58.60	56.23	56.89	56.54	55.54	53.99	55.95	56.43	55.50	55.86	53.74	53.31
TiO2	0.08	0.11	0.07	0.13	0.08	0.11	0.19	0.23	0.15	0.14	0.16	0.26	0.18	0.17
Al2O3	1.48	1.64	0.82	1.26	1.54	1.35	1.02	0.90	1.01	1.22	0.95	1.23	1.02	0.82
Cr2O3	0.57	0.54	0.39	0.51	0.55	0.56	0.16	0.05	0.15	0.52	0.21	0.05	0.26	0.14
FeO*	7.44	9.41	5.16	10.67	8.93	10.23	13.76	20.62	13.45	10.49	14.86	13.67	18.18	22.94
MnO	0.18	0.22	0.13	0.24	0.21	0.23	0.29	0.41	0.30	0.24	0.34	0.31	0.32	0.40
MgO	31.92	30.72	35.37	30.52	30.77	30.28	27.54	23.12	28.59	30.47	26.88	28.66	24.80	21.65
CaO	1.70	1.29	0.51	0.87	1.86	1.38	2.21	1.33	1.00	1.14	1.50	1.10	1.24	1.04
Na2O	0.02	0.01	0.03	0.01	0.02	0.01	0.03	0.04	0.02	0.03	0.02	0.01	0.02	0.03
K2O	0.01	0.01	0.01	0.01	0.02	0.01	0.01	0.01	0.01	0.01	0.01	0.00	0.01	0.00
Totale	100.56	100.84	101.07	100.44	100.86	100.71	100.74	100.70	100.62	100.69	100.44	101.16	99.77	100.50
Fe3+	0.00	0.00	0.000	0.00	0.00	0.00	0.00	0.00	0.00	0.00	0.00	0.00	0.01	0.00
Fe2+	0.22	0.27	0.146	0.31	0.26	0.30	0.41	0.63	0.40	0.31	0.44	0.40	0.55	0.71
Wo	3.29	2.52	0.94	1.68	3.59	2.69	4.33	2.68	1.95	2.20	2.97	2.14	2.47	2.11
En	85.46	83.17	91.47	82.17	82.84	81.77	74.65	64.75	77.54	81.88	74.01	77.17	69.05	61.33
Fs	11.18	14.29	7.48	16.12	13.48	15.49	20.92	32.41	20.45	15.81	22.95	20.64	28.39	36.45
mg**	88.43	85.34	92.44	83.60	86.00	84.07	78.12	66.64	79.13	83.82	76.33	78.89	70.87	62.72

clinopyroxene

	St3	St4	St5	St7	St8	St9	St10	St12	St13	St14	St16	St18	St19	St20
SiO2	54.54	53.56	53.19	54.12	53.45	52.73	52.58	53.92	52.60	53.27	52.81	52.60	52.43	52.76
TiO2	0.18	0.28	0.39	0.16	0.43	0.46	0.46	0.32	0.42	0.38	0.56	0.56	0.91	0.46
Al2O3	1.81	2.10	2.69	1.67	1.82	2.10	1.74	1.68	1.94	1.74	2.29	2.25	2.71	1.73
Cr2O3	0.99	0.92	1.17	1.12	0.34	0.08	0.06	0.34	0.26	0.34	0.10	0.17	0.34	0.39
FeO*	2.41	4.40	3.80	3.77	5.70	8.02	9.08	5.72	8.13	6.73	6.03	7.46	5.90	6.88
MnO	0.05	0.10	0.13	0.05	0.17	0.21	0.24	0.14	0.20	0.17	0.18	0.19	0.14	0.16
MgO	17.22	16.29	16.38	16.38	15.61	14.43	14.02	16.14	14.69	15.60	15.62	14.83	15.72	15.31
CaO	22.97	22.79	22.39	23.11	22.71	21.61	22.19	22.10	21.89	21.81	22.36	22.33	22.07	22.29
Na2O	0.47	0.35	0.48	0.29	0.27	0.21	0.21	0.20	0.28	0.23	0.28	0.24	0.31	0.20
K2O	0.00	0.02	0.01	0.00	0.00	0.01	0.01	0.00	0.01	0.02	0.01	0.00	0.00	0.02
Totale	100.65	100.81	100.64	100.66	100.51	99.85	100.57	100.57	100.43	100.31	100.24	100.62	100.52	100.19
Fe^{3+}	0.00	0.00	0.01	0.00	0.00	0.01	0.01	0.00	0.02	0.00	0.02	0.02	0.01	0.02
Fe^{2+}	0.07	0.13	0.11	0.11	0.17	0.24	0.27	0.17	0.23	0.21	0.17	0.21	0.17	0.19
Wo	46.25	46.02	45.67	46.81	45.99	44.69	45.13	44.73	44.50	44.34	45.35	45.36	44.93	45.19

En	48.25	45.78	46.50	46.16	44.00	41.56	39.68	45.47	41.56	44.13	44.08	41.93	44.54	43.21
Fs	3.79	6.93	6.05	5.95	9.01	12.95	14.41	9.05	12.91	10.68	9.55	11.83	9.37	10.89
mg**	92.72	86.86	88.48	88.58	83.01	76.24	73.36	83.50	76.34	80.55	82.19	77.98	82.62	79.88

plagioclase

	St2	St4	St5	St7	St8	St9	St10	St12	St13	St14	St16	St18	St19	St20	St25
SiO2	51.31	49.28	50.07	50.53	49.07	48.57	49.15	48.82	48.68	48.81	48.33	48.98	47.84	44.18	48.80
TiO2	0.05	0.02	0.03	0.03	0.03	0.00	0.03	0.03	0.03	0.02	0.00	0.03	0.03	0.04	0.00
Al2O3	31.03	32.03	31.68	31.36	32.78	32.75	31.96	32.73	32.28	32.53	33.18	32.19	33.38	32.35	33.10
FeO	0.16	0.17	0.14	0.33	0.36	0.47	0.50	0.37	0.36	0.35	0.40	0.44	0.34	0.35	0.19
CaO	14.61	16.10	15.62	14.97	16.19	16.17	16.26	16.38	16.32	16.22	16.42	16.34	16.97	19.67	16.58
Na2O	3.28	2.50	2.80	2.95	2.21	2.27	2.39	2.12	2.30	2.28	2.06	2.36	1.80	1.33	2.13
K2O	0.12	0.13	0.07	0.14	0.10	0.08	0.08	0.07	0.09	0.10	0.06	0.07	0.07	0.01	0.08
Totale	100.56	100.23	100.41	100.31	100.75	100.36	100.37	100.52	100.06	100.31	100.45	100.40	100.41	99.48	100.89
Fe^{2+}	0.01	0.01	0.01	0.01	0.01	0.02	0.02	0.01	0.01	0.01	0.02	0.02	0.01	0.08	0.01
Ab %	28.70	21.78	24.38	26.08	19.67	20.16	20.92	18.89	20.21	20.19	18.45	20.60	16.00	10.96	18.75
An %	70.61	77.50	75.21	73.08	79.74	79.39	78.60	80.72	79.27	79.23	81.19	78.99	83.61	89.00	80.80
Or %	0.69	0.72	0.41	0.84	0.59	0.45	0.48	0.40	0.52	0.58	0.36	0.41	0.39	0.04	0.45

olivine

	St1	St2	St5	St6	St16	St19
SiO2	41.36	40.77	40.88	41.42	39.33	39.73
TiO2	0.02	0.02	0.01	0.01	0.02	0.04
Al2O3	0.00	0.01	0.01	0.01	0.01	0.27
FeO	11.70	14.97	14.67	11.51	21.44	20.69
MnO	0.18	0.22	0.20	0.13	0.29	0.28
MgO	47.28	44.40	44.92	47.74	39.75	39.47
CaO	0.03	0.03	0.04	0.03	0.04	0.33
Totale	100.57	100.41	100.73	100.87	100.89	100.81
Fe^{2+}	0.24	0.31	0.30	0.24	0.46	0.44
Fo	87.65	83.90	84.34	87.97	76.53	77.05
Fa	12.16	15.87	15.45	11.90	23.15	22.64
mg**	87.81	84.10	84.52	88.08	76.77	77.29

Table 3 - Microprobe average measurements of mineral phases present in our Stillwater Complex samples. Opx,cpx recalculated on base of 6 oxygen, Pl on base of 8 oxygen, Ol on base of 4 oxygen. Fe^{2+} and Fe^{3+} are recalculated in a.f.u. StC11 and St17 where not measured, those

samples are from the same layers and with very similar characteristics of StC9 and StC19, respectively.